PRODUCTION AND CHARACTERIZATION OF SIMPLE, FACE-CENTERED AND DIAMOND CUBIC LATTICES BY FUSED DEPOSITION MODELING USING POLYLACTIC ACID

A THESIS SUBMITTED TO
THE GRADUATE SCHOOL OF NATURAL AND APPLIED SCIENCES
OF
MIDDLE EAST TECHNICAL UNIVERSITY

BY
ARİF DÖNMEZ

IN PARTIAL FULFILLMENT OF THE REQUIREMENTS
FOR
THE DEGREE OF MASTER OF SCIENCE
IN
ENGINEERING SCIENCES

AUGUST 2022

Approval of the thesis:

PRODUCTION AND CHARACTERIZATION OF SIMPLE, FACE-CENTERED AND DIAMOND CUBIC LATTICES BY FUSED DEPOSITION MODELING USING POLYLACTIC ACID

submitted by **ARİF DÖNMEZ** in partial fulfillment of the requirements for the degree of **Master of Science in Engineering Sciences, Middle East Technical University** by,

Prof. Dr. Halil Kalıpçılar
Dean, Graduate School of **Natural and Applied Sciences** _____

Prof. Dr. Murat Dicleli
Head of the Department, **Engineering Sciences** _____

Prof. Dr. Zafer Evis
Supervisor, **Engineering Sciences, METU** _____

Examining Committee Members:

Prof. Dr. Fahrettin Öztürk
Mechanical Engineering, Ankara Yıldırım Beyazıt Uni. _____

Prof. Dr. Zafer Evis
Engineering Sciences, METU _____

Assoc. Prof. Dr. Onur Behzat Tokdemir
Civil Engineering, ITU _____

Asst. Prof. Dr. Yasin Sarıkavak
Mechanical Engineering, Ankara Yıldırım Beyazıt Uni. _____

Prof. Dr. Dilek Keskin
Engineering Sciences, METU _____

Date: 22.08.2022

I hereby declare that all information in this document has been obtained and presented in accordance with academic rules and ethical conduct. I also declare that, as required by these rules and conduct, I have fully cited and referenced all material and results that are not original to this work.

Name, Last name: Arif Dönmez

Signature:

ABSTRACT

PRODUCTION AND CHARACTERIZATION OF SIMPLE, FACE-CENTERED AND DIAMOND CUBIC LATTICES BY FUSED DEPOSITION MODELING USING POLYLACTIC ACID

Dönmez, Arif
Master of Science, Engineering Sciences
Supervisor: Prof. Dr. Zafer Evis

August 2022, 74 pages

This thesis focuses on the characterization of simple, face-centered and diamond cubic lattices produced by fused deposition modeling (FDM) using polylactic acid (PLA) under uniaxial compression loading condition. Four design parameters were set for each cubic lattice: with radius, without radius, hollow truss, and hollow and with radius. Test items were manufactured for all designed structures. Since changing the manufacturing direction changes the mechanical properties of cubic lattices, the tests were done both through the manufacturing and non-manufacturing directions of the cubic lattices. Based on the data obtained from tests, stress strain diagrams were prepared for each parameter and the manufacturing direction. Nonlinear material and nonlinear geometrical finite element analysis were performed and stress strain diagrams were created based on the results of the finite element analysis. Also, strength and weight reduction calculations were done to determine the ultimate tensile strength point for each lattice type. As those calculations show, manufacturing direction of cubic lattices has a strong effect on mechanical properties of simple, face-centered and diamond cubic lattices under uniaxial compression loading condition.

Keywords: FDM method, simple, face-centered and diamond cubic lattices

ÖZ

POLİLAKTİK ASİT'TEN ERİYİK YIĞMA YÖNTEMİYLE ÜRETİLEN BASİT, YÜZEY MERKEZLİ VE ELMAS KÜBİK YAPILARIN KARAKTERİZASYONU

Dönmez, Arif

Yüksek Lisans, Mühendislik Bilimleri

Tez Yöneticisi: Prof. Dr. Zafer Evis

Ağustos 2022, 74 sayfa

Bu tezde, polilaktik asit'ten üretilen basit, yüzey merkezli ve elmas kübik yapıların basma yükü altındaki karakterizasyonu yapılmıştır. Temel olarak dört adet tasarım parametresi kullanılmıştır. Bunlar, kirişlerin kenarlarında radyus olması, kirişlerin kenarlarında radyus olmaması, kirişlerin içlerinin boş olması ve kirişlerin içlerinin boş olup birleştikleri yerlerde radyus olmasıdır. Tasarlanan tüm yapıların basma testleri yapılmıştır. Üretim yönüyle yapılan basma yükü mekanik özellikleri ile üretim yönüne dik yapılan basma yükü mekanik özellikleri birbirinden farklılık gösterdiğinden, basma testleri üretim yönüyle aynı ve üretim yönüne dik olmak üzere iki kez tekrarlanmıştır. Testler yapıldıktan sonra, elde edilen yer değiştirme ve yük bilgilerine dayalı olarak stres ve gerginlik diyagramları oluşturulmuştur ve bu diyagramlar her tasarım parametresi ve üretim yönüne göre tekrarlanıp hesaplanmıştır. Sonlu elemanlar yöntemi kullanılarak testten elde edilen verilerle malzeme değerleri elde edilmiş, daha sonra bu bilgiler sonlu elemanlar programına girilerek bilgisayar ortamında simülasyonlar yapılmıştır. Yapılan simülasyonlarda doğrusal olmayan malzeme bilgisi ve doğrusal olmayan geometrik bilgiler kullanılmıştır. Tüm tasarım çeşitleri ve parametreleri için dayanım ve ağırlık azaltma hesapları yapılmıştır. Bu hesaplamalardan, parçaların akma noktalarının üretim yönüne göre birbirlerinden farklılık gösterdikleri gözlemlenmiştir.

Anahtar kelimeler: Eriyik yığma yöntemi, basit, yüzey merkezli ve elmas kübik latisler

To my grandmother

ACKNOWLEDGMENTS

I would like to thank my supervisor Prof. Dr. Zafer Evis for his dedication, support, and guidance throughout this study. I am grateful to him for the invaluable feedback he has provided and for his allocation and arrangement of time, which helped me a lot to complete this study in the most time efficient manner.

I would like to express my gratitude to my colleague Okan Türe for the finite element model he created as well as for his constructive comments throughout my study.

My thanks are due to Turkish Aerospace Inc. for producing the mechanical designs as well as for supplying the materials, design programs and analysis tools.

I would also like to thank Engineering Sciences Department PhD. student Hossein Jodati for his guidance concerning the use of the mechanical test laboratory.

Finally, I owe special thanks to my mother, grandmother and grandfather for their support, encouragement, and patience.

TABLE OF CONTENTS

ABSTRACT v

ÖZ v

ACKNOWLEDGEMENTS ix

TABLE OF CONTENTS xi

LIST OF TABLES xiii

LIST OF FIGURES xv

LIST OF ABBREVIATIONS xvii

LIST OF SYMBOLS xix

1. INTRODUCTION 1

1.1 Overview 1
1.2 Lattice structures 2
1.3 Problem statement 4
1.4 Objectives of this thesis 4
1.5 Significance of the study 5

2. LITERATURE REVIEW 7

2.1 Additive manufacturing methods and materials 7
2.2 Fused deposition modeling (FDM) 9
2.3 Cellular materials 11
2.3.1 Strut-based lattice structures 12
2.3.2 Triply periodic minimal surface lattice structures 13
2.3.3 Shell lattice structures 14
2.3.4 Simple, face-centered and diamond cubic lattice structures 15
2.3.5 Additive manufacturing of lattice structures 20
2.3.6 Design and optimization of lattice structures 23
2.3.7 Analytical analysis of lattice structures 26
2.3.8 Finite element analysis of cubic lattices 27

3. MATERIALS AND METHODS 29

3.1 Materials 29
3.1.1 Characterization of PLA with FTIR, XRD and DSC methods 29
3.2 Production of lattice structures by FDM 30

3.3 Mechanical testing 32
3.4 Finite element analysis 33
3.4.1 One dimensional element CBAR 33
3.4.2 Modeling of cubic lattices with CBAR structural element method 36

4. RESULTS & DISCUSSION 37

4.1 Characterization of PLA with FTIR, XRD and TGA methods 37
4.1.1 Characterization of PLA with FTIR method 37
4.1.2 Characterization of PLA with XRD method 38
4.1.3 Characterization of PLA with DSC method 39
4.2 Simple cubic lattice 40
4.3 Face-centered cubic lattice 49
4.4 Diamond cubic lattice 60

5. CONCLUSION 69

REFERENCES 71

LIST OF TABLES

TABLES

Table 3.1. Identification of lattice types and their explanations..... 31
Table 3.2. FDM parameter types and their manufacturing parameters..... 32
Table 3.3. Analytical calculations of solid and hollow trusses 35
Table 4.1. Strength and weight reduction rate calculation for simple cubic lattices. 45
Table 4.2. Strength and weight reduction rate calculation for face-centered cubic lattices 54
Table 4.3. Strength and weight reduction rate calculation for diamond cubic lattices 65

LIST OF FIGURES

FIGURES

Figure 2.1. Commonly used areas for AM methods (Bikas et al., 2016)..... 7
Figure 2.2. Fused deposition modeling (Ahn et al., 2002)..... 10
Figure 2.3. Strut-based structures: (a) BCC, (b) BCCZ, (c) FCC, (d) FCCZ, (e) Cubic, (f) Octet-truss, (g) Diamond (Maconachie et al., 2019)..... 13
Figure 2.4. Triply periodic minimal surface unit cells: a) Scheon gyroid, b) Schwarz diamond and c) Neovius (Maconachie et al., 2019)..... 14
Figure 2.5. Solid mesh of a unit cell (Zhou et al., 2021)..... 16
Figure 2.6. Intersection points of octahedral truss structure (Kaur et al., 2017)..... 17
Figure 2.7. Displacement behaviors of stretching-dominated and bending dominated trusses: a) stretching-dominated displacement behavior of octet truss, b) bending-dominated displacement behavior of BCC (Sun et al., 2021a)..... 18
Figure 2.8. Ashby-Gibson model (Peng, 2020) 26
Figure 3.1. a) Solid truss section, b) Hollow truss section..... 34
Figure 3.2. a) Simple cubic lattice, b) Face-centered cubic lattice, c) Diamond cubic lattice..... 36
Figure 4.1. FTIR result of PLA 38
Figure 4.2. XRD result of PLA 39
Figure 4.3. DSC result of PLA..... 40
Figure 4.4. a) SC-WR-M, b) SC-R-M, c) SC-WR-H-M, d) SC-R-H-M 42
Figure 4.5. a) SC-WR-NM, b) SC-R-NM, c) SC-WR-H-NM, d) SC-R-H-NM..... 43
Figure 4.6. a) SC fem modeling before compression load, b) SC fem modeling after compression load..... 46
Figure 4.7. a) SC before the test, b) SC during the test, d) SC after the test..... 46
Figure 4.8. SC first eigenvalue mode..... 47
Figure 4.9. SC second eigenvalue mode 48
Figure 4.10. a) SC-WR, b) SC-R, c) SC-WR-H, d) SC-R-H, e) SC-WR-MD failure, f) SC-R-M failure, g) SC-WR-H-M failure, h) SC-R-H-M failure, i) SC-WR-NM failure, j) SC-R-NM failure, k) SC-WR-H-NM failure, l) SC-R-H-NM failure..... 49
Figure 4.11. a) FC-WR-M, b) FC-R-M, c) FC-WR-H-M, d) FC-R-H-M 51
Figure 4.12. a) FC-WR-NM, b) FC-R-NM, c) FC-WR-H-NM, d) FC-R-H-NM..... 52
Figure 4.13. a) FC fem modeling before compression load, b) FC fem modeling after compression load..... 55
Figure 4.14. a) FC before the test, b) FC during the test, d) FC after the test..... 55
Figure 4.15. FC first eigenvalue mode..... 56
Figure 4.16. FC second eigenvalue mode 57
Figure 4.17. FC third eigenvalue mode..... 57
Figure 4.18. FC fourth eigenvalue mode..... 58
Figure 4.19. a) FC-WR, b) FC-R, c) FC-WR-H, d) FC-R-H, e) FC-WR-MD failure, f) FC-R-M failure, g) FC-WR-H-M failure, h) FC-R-H-M failure, i) FC-WR-NM failure, j) FC-R-NM failure, k) FC-WR-H-NM failure, l) FC-R-H-NM failure..... 59
Figure 4.20. a) DC-WR-M, b) DC-R-M, c) DC-WR-H-M, d) DC-R-H-M..... 62
Figure 4.21. a) DC-WR-NM, b) DC-R-NM, c) DC-WR-H-NM, d) DC-R-H-NM .. 63

Figure 4.22. a) DC fem modeling before compression load, b) DC fem modeling after compression load 66
Figure 4.23. a) DC before the test, b) DC during the test, d) DC after the test..... 66
Figure 4.24. DC eigenvalue mode..... 67
Figure 4.25. a) DC-WR, b) DC-R, c) DC-WR-H, d) DC-R-H, e) DC-WR-MD failure, f) DC-R-M failure, g) DC-WR-H-M failure, h) DC-R-H-M failure, i) DC-WR-NM failure, j) DC-R-NM failure, k) DC-WR-H-NM failure, l) DC-R-H-NM failure 68

LIST OF ABBREVIATIONS

ABBREVIATIONS	
PLA	Polylactic Acid
FDM	Fused Deposition Modeling
AM	Additive Manufacturing
SC-WR-NM	Simple Cubic Lattice Without Radius and Non-manufacturing Direction
SC-WR-M	Simple Cubic Lattice Without Radius Manufacturing Direction
SC-R-NM	Simple Cubic Lattice With Radius Non-manufacturing Direction
SC-R-M	Simple Cubic Lattice With Radius Manufacturing Direction
SC-WR-H-NM	Simple Cubic Lattice Without Radius and Hollow Non-manufacturing Direction
SC-WR-H-M	Simple Cubic Lattice Without Radius Hollow Manufacturing Direction
SC-R-H-NM	Simple Cubic Lattice With Radius and Hollow and Non-manufacturing Direction
SC-R-H-M	Simple Cubic Lattice With Radius and Hollow and Manufacturing Direction
FC-WR-NM	Face-Centered Cubic Lattice Without Radius Non-manufacturing Direction
FC-WR-M	Face-Centered Cubic Lattice Without Radius and Manufacturing Direction
FC-R-NM	Face-Centered Cubic Lattice With Radius and Non-manufacturing Direction
FC-R-M	Face-Centered Cubic Lattice With Radius Manufacturing Direction
FC-WR-H-NM	Face-Centered Cubic Lattice Without Radius and Hollow Non-manufacturing Direction
FC-WR-H-M	Face-Centered Cubic Lattice Without Radius and Hollow Manufacturing Direction
FC-R-H-NM	Face-Centered Cubic Lattice With Radius Hollow Non-manufacturing Direction

FC-R-H-M	Face-Centered Cubic Lattice With Radius and Hollow and Manufacturing Direction
DC-WR-NM	Diamond Cubic Lattice Without Radius Non-manufacturing Direction
DC-WR-M	Diamond Cubic Lattice Without Radius and Manufacturing Direction
DC-R-NM	Diamond Cubic Lattice With Radius and Non-manufacturing Direction
DC-R-M	Diamond Cubic Lattice With Radius Manufacturing Direction
DC-WR-H-NM	Diamond Cubic Lattice Without Radius Hollow Non-manufacturing Direction
DC-WR-H-M	Diamond Cubic Lattice Without Radius and Hollow and Manufacturing Direction
DC-R-H-NM	Diamond Cubic Lattice With Radius and Hollow Non-manufacturing Direction
DC-R-H-M	Diamond Cubic Lattice With Radius Hollow Manufacturing Direction

LIST OF SYMBOLS

SYMBOLS

°	Degree
°C	The degree Celsius
MPa	Megapascal
$\in_{xx}$	Strain value of x direction of material
$\in_{yy}$	Strain value of y direction of material
$\in_{zz}$	Strain value of z direction of material
E_s	Elastic modulus of solid material
E^*	Elastic modulus of cellular material
ρ_s	Density of solid material
ρ^*	Density of cellular material

CHAPTER 1

1. INTRODUCTION

1.1 Overview

In this thesis, simple, face-centered and diamond cubic lattices were manufactured by the fused deposition modeling (FDM) method using polylactic acid (PLA) and they were characterized by conducting structural and mechanical tests.

Additive Manufacturing (AM) is the ejection of thin layers of material upon each other to generate three dimensional (3D) models. The AM method has been developed in the last 50 years (Pereira et al., 2019). Layer thickness is in the range of 0.0254 to 2.54 millimeters (Attaran, 2017). The AM method has been widely used in aerospace, automotive, biomedical industries and some other fields such as architectural design and digital art. Also, the method is used for rapid prototyping to reduce the time to create a 3D model.

The AM method offers some advantages over traditional manufacturing methods. One of them is that 3D parts can be designed and manufactured more easily than through traditional methods. Another advantage is that AM does not require tooling time, and this enables rapid prototyping. Moreover, AM is used for the transition of a Computer Aided Design (CAD) file to three-dimensional physical model. In this process, the CAD file is converted to a stereolithography (STL) file and then the manufacturing step begins. It can also be defined as a process of adding materials layer by layer to make objects from a 3D model data. During the process, there are three phases of material which are first fused, then cooled, and finally solidified to create 3D models. The method has some disadvantages, however. Limited materials, poor repeatability, and poor part accuracy are some of them.

1.2 Lattice Structures

Lattice structures can be defined as objects which repeat themselves as a unit cell and get interconnected in three dimensions in nature (Helou & Kara, 2018). They are generally composed of truss structures and have minimal section area of surfaces. Those lattice structures have advantages over traditional structural elements. Decreasing the amount of material inside the structure and having a good strength property while reducing the weight are two important advantages which lattice structures offer. These structures also have energy absorption, acoustic, vibration damper, and thermal management properties (Helou & Kara, 2018). Due to these advantages and properties lattice structures can be used for different engineering applications.

Moreover, hollow truss structures can carry more loads than solid fill structures since the second moment of area of hollow truss is greater than that of a solid truss. Hollow lattice structures can be used for energy-absorption systems, and they are preferred over honeycombs because of their density. If structures can be filled with rubber-like materials their Young's modulus increases and this leads to an increased load capacity under loading condition (Helou & Kara, 2018).

Generally, lattice structures have two distinctly different topologies which are stochastic and periodic. Stochastic lattice structures' molecules are distributed randomly. Some examples of stochastic lattice structures are bone structures, cellulose aggregates in wood or collagen aggregates in cartilage (Helou & Kara, 2018). The disadvantage of stochastic lattice structures is that their analysis and failure modes cannot be predicted precisely. In periodic lattice structures, however, molecules are diffused according to an order. Honeycomb topology, for example, is a type of periodic lattice structure. According to the literature, stochastic type of lattice structures has so many disadvantages because of their randomly distributed behavior (Helou & Kara, 2018).

The definition of lattice structure changes since there are different application areas such as structural and civil engineering, biological and materials sciences, and crystallography. Lattice structures can be defined as space-filling or close packing

structures that have three dimension and that can repeat themselves through in any direction (Helou & Kara, 2018). A lattice structure is designed with a reference to a plane or axis and there is no restriction for the type of coordinate system and deposition layout.

Furthermore, lattice structures are the type of cellular structures, and they can be created by different materials. Honeycomb is an example for the cellular type structures and its topological geometry is mimicked from natural honeycomb. Also, those structures are useful in different industrial areas. To illustrate, honeycomb is an attractive option to use in aerospace industries since it is light-weight and very resistant against pure bending conditions. There are also different natural cellular structures, and they can be produced with FDM. Metallic foams are the type of cellular structures which can be produced by injecting gas or mixing a foaming agent into molten metal (Maconachie et al., 2019). Although manufacturing them is not expensive, they are not preferred since molecular random behavior inside the structure causes anisotropy and this changes the mechanical properties. However, lattice structures are different from other foams such as metallic foams in terms of the regularly repeating structure of their unit cells.

Cellular materials can be defined as interconnected network of struts or plates (Maconachie et al., 2019). The main structural elements of lattice structures are frames, trusses or beams in micrometer or millimeter scale. Classical mechanical analysis methods are useful for lattice structures but the difference between large scale strut model and lattice model is that lattices have their own material properties which are related with their material printing shapes (Maconachie et al., 2019).

Lattice structures are classified based on their mechanical response as bending-dominated or stretch-dominated (Maconachie et al., 2019). Bending-dominated lattice structures are resistant against pure bending load condition and stretch-dominated lattice structures are invulnerable against tension or compression load condition. The cell topology of lattice structures is designed in line with the mechanical behavior desired. The cell topology of lattice structures can be categorized as strut-based or triply periodic minimal surfaces (TPMS) (Maconachie et al., 2019).

1.3 Problem Statement

Manufacturing mechanical parts by using AM methods offers great benefits for aerospace, biomedical and other engineering applications. Lattice structures can show good mechanical behavior under compression loading conditions. Simple, face-centered and diamond cubic lattices have better mechanical properties under compressive loads when compared, for example, with metallic sandwich panels. They are lightweight and their ultimate tensile strength points are higher. Cubic lattices cannot be manufactured with traditional methods and polymer materials such as PLA can be used with AM methods.

1.4 Objectives of This Thesis

The main objective of this thesis is to characterize the simple, face-centered and diamond cubic lattices under compressive loading conditions.

The specific objectives are summarized as follows:

1. To design and manufacture simple, face-centered and diamond cubic lattices which have with radius, without radius, hollow and hollow and with radius truss parameters by using the FDM method.
2. To find out how these lattices perform under compression load condition by obtaining the stress-strain curves through various tests.
3. To characterize polylactic acid by employing Fourier-transform infrared spectroscopy, X-Ray Diffraction Analysis and Differential Scanning Calorimetry.
4. To prepare finite element models for simple, face-centered and diamond cubic lattices which have with radius, without radius, hollow and hollow and with radius truss parameters, to obtain stress-strain curve diagrams from finite element models and to see if they correlate with the test results.

1.5 Significance of the Study

In this study, simple, face-centered and diamond cubic lattice structures with different parameters (radius and hollow truss) were produced by the FDM method and their performance under compression loading condition was investigated. The behavior of cubic lattice structures under compression load has been subjected to many studies. However, hollow truss and radius parameters have not been studied. Aim of this study is to minimize weight of the cubic lattice structures according to compression load and this is done by adding radii at the junction points of trusses and removing material from truss centers which is hollow truss parameter. Furthermore, there are two methods to increase strength of the cubic lattices while decreasing the weight of the structure. First method is that adding radii at the junction points of trusses and second method is that removing the material from truss centers.

CHAPTER 2

2. LITERATURE REVIEW

2.1 Additive manufacturing methods and materials

There are different AM methods, and they differ from each other in terms of the deposition way used to create 3D models. Mainly, there are four different AM methods, which are selective laser melting (SLM), selective laser sintering (SLS), FDM, and stereolithography (SLA). AM methods have various application areas. In Figure 2.1, the application areas of the AM method are shown.

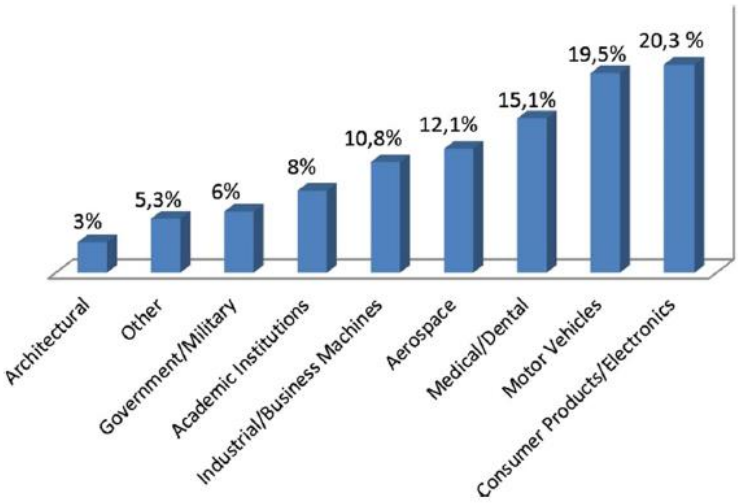

Figure 2.1. Commonly used areas for AM methods (Bikas et al., 2016)

AM processes are distributed as laser based, extrusion thermal, material jetting, material adhesion, and electron beam. In laser based processes, material can be melted and solidified with using laser and this leads to a decrease in power. There are two categories for laser-based processes, which are laser polymerization and laser melting. In laser polymerization, liquid photosensitive material solidifies under laser source. Laser polymerization processes are not recommended for structural parts

since they show low strength values and are generally used for prototyping. Stereolithography (SLA), solid ground curing (SGC), liquid thermal polymerization (LTP), beam interference solidification (BIS), and holographic interference solidification (HIS) are types of the laser polymerization process (Bikas et al., 2016). In laser melting, laser beam contributes to the melting of the fine powder and then the material cools down and solidifies to final part. SLS, SLM, direct metal laser sintering (DMLS), laser engineered net shaping (LENS), direct metal deposition (DMD), laser powder deposition (LPD), and selective laser cladding (SLC) are types of laser melting processes (Bikas et al., 2016).

In the material extrusion technique, nozzle heats the material in order to soften or melt it. After the melting operation, the material comes down from the nozzle and the nozzle travels the table according to a three-dimensional drawing model. Then the material solidifies and creates the 3D model. One common material extrusion technique is FDM and another is robocasting (Bikas et al., 2016).

Material jetting processes use nozzle to spray material, which can be molten or adhesive. The operating process of material jetting is nearly the same as laser-melting processes. However, the difference between the laser-melting and material jetting processes is that phase change is not allowed in material jetting process. Three-dimensional printing (3DP), Inkjet printing (IJP), multijet modelling (MJM), ballistic particle manufacturing (BPM) and thermojet all belong to material jetting process types (Bikas et al., 2016).

Adhesive-based processes are not preferred as the operating principle is more complicated than that of other processes. The operating principle includes a cutter which is usually a laser to cut a thin film of paper or plastic. The film of paper or plastic flow moves down onto previous one to obtain the desired shape. Laminated object manufacturing (LOM) and solid foil polymerization (SFP) are the types of adhesive-based processes (Bikas et al., 2016).

Electron beam processes are almost the same as laser-melting processes except for the fact that electron beam is used instead of laser beam in electron beam processes. Electron beam manufacturing (EBM) is a new process and is one of the types of electron beam processes (Bikas et al., 2016). There are different material types used

in AM, and polymers are one of them. Thermoplastics and thermosets are two types of polymers. Thermoplastic polymers are used in material extrusion and powder bed fusion processes, and they differ from each other in that amorphous thermoplastic is used for material extrusion and semicrystalline polymers are used for powder bed fusion. Thermosets are photopolymer materials used in the AM method. Metals are other material types for AM processes. In order to produce metal parts, powder bed fusion and directed energy deposition are two different AM processes that are mainly employed. Commonly used metals are pure titanium, Ti6AL4V, 316L stainless steel, 17-4PH stainless steel, 18Ni300 maraging steel, AlSi10Mg, and CoCrMo625 (Bourell et al., 2017). Ceramics are also used in AM processes but they are more difficult to shape than polymers and metals because of their high melting points and brittleness. Obtaining the full density of ceramic is a challenge while alumina and its alloys can be directly processed using directed energy deposition (Bourell et al., 2017). Polymer, metal, and ceramic matrix composites are three different composite materials used in the AM method. Convenient bonding between the matrix and embedded phase is the most important factor for the transfer of load and corrosion resistance for composite materials in AM. Material extrusion processes lead to heterogeneous layering of material and this results in low mechanical properties for composite materials.

2.2 Fused deposition modeling (FDM)

AM methods make it possible to produce three dimensional mechanical parts more rapidly than traditional manufacturing methods, which has led to the development of Rapid Prototyping (RP). FDM is one of these methods. In the FDM method, molten filament such as ABS or PLA is deposited through the printer's table according to the design of a part. In the working scheme of FDM, firstly, a 3D model is designed and then the model is converted into the STL file format. Secondly, STL is imported by slicer programs and parts are sliced into many sections in line with designer requests. Lastly, the sliced 3D model is plugged into a three-dimensional printer and parts can be produced. While producing parts, ABS or PLA filament is fed through a heating element and becomes semi-molten. Semi-molten material comes from a

nozzle and is deposited layer by layer to create the 3D part. The nozzle moves through the X and Y plane of 3D-printing table according to the part geometry and the Z plane is used to print the next layer of the 3D part. The FDM machine uses a second nozzle to create support structures, which is needed when a geometrical part inside is hollow or gaps exist between the main structures of part geometry. To produce support structures, there should be an overhang angle that is less than 45 degrees from horizontal, and if the angle is more than 45 degrees, then the structure tends to fall. The FDM machine prints the material in a directional way and this leads to anisotropy. Anisotropy means the material doesn't have the same mechanical properties in all its directions.

There are several experiments done to determine which direction of fused deposition method yields structures with good mechanical properties, and they similarly showed that the printing way or the deposition direction has a strong effect on the mechanical performance of 3D geometries (Bourell et al., 2017). In Figure 2.2, the working mechanism of the FDM method is shown.

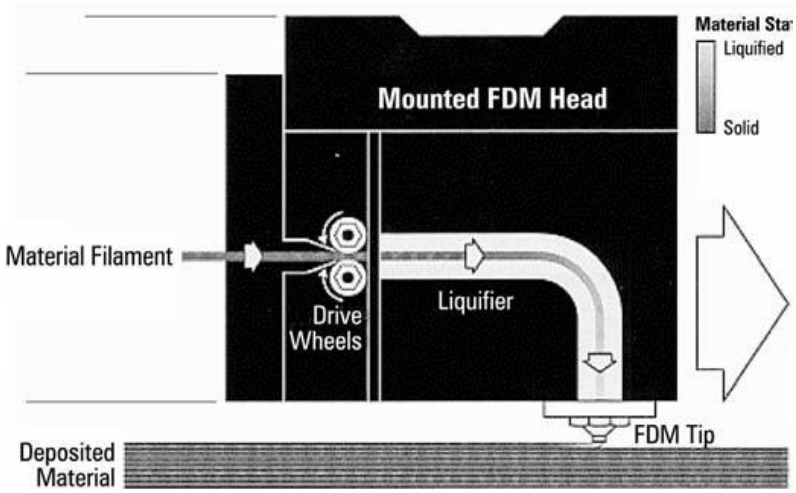

Figure 2.2. Fused deposition modeling (Ahn et al., 2002)

There are some building parameter types which are important for part geometry since they have strong effect on mechanical properties of 3D geometry.

The first one is bead width, which is the thickness of the bead or the road FDM nozzle prints. Its thickness varies from 0.3 mm to 1 mm for the FDM machine (Ahn et al., 2002). The second one is the air gap, which is the distance between the beads

of material. Zero air gap value means each bead touches closely to each other. If someone wants to obtain dense structure, the air gap value should be negative. When positive gap values are used, the gap between beads increases and this results in manufacturing weak structures. The third one is the building temperature, which has an effect on the viscosity of molten material. The last one is raster orientation, which refers to the direction of the beads of material. While bead width, air gap, building temperature and raster orientation have a strong impact on mechanical properties, factors such as envelope temperature, slice height and nozzle diameter do not have any significant effect on the mechanical properties of part geometries.

Envelope temperature is the air temperature value around the material. Envelope temperature constantly changes while producing geometrical parts and fixing envelope temperature is not easy. As for slice height, the thickness should be the same for each layer to obtain homogenous material density and mechanical properties. Nozzle diameter does not have primary effect on mechanical properties because if the diameter is smaller than the desired value, the designer can increase the printing time and can obtain similar material properties.

Consequently, the FDM method is one type of the AM processes, and polymers such as PLA and ABS are generally used as FDM method materials. While using FDM machines, building temperature, air gap and bead width are important building parameters to achieve the desired mechanical properties (Ahn et al., 2002).

2.3 Cellular materials

Cell structures can be designed and manufactured with the aid of additive manufacturing technologies and single piece of material can be added to the desired position. Lattice structures have various benefits. They are lightweight, have good absorption properties and are good heat exchangers (Savio et al., 2018). Therefore, they find use in various industrial applications. The aerospace and biomedical industries are only a few no name.

There are several cellular material taxonomies in literature. They are disordered cellular structures which have different size and geometrical lattices. They can be

periodic and pseudo periodic (Savio et al., 2018). Regular, pseudorandom, and random structures are the three types of cellular structures that define shapes. Regular cellular materials repeat themselves through entire volume. Pseudorandom structures can be created by changing both size and geometry, while random cellular materials have random size, geometry, and shape (Savio et al., 2018). Apart from these three types, there are foam structures and they can be manufactured with traditional manufacturing methods and additive manufacturing technologies.

Cellular materials are also classified according to cell topology. Open cell topology means that fluid can penetrate all the pores of a structure. Close cell topology means that fluid cannot access porous structure (Savio et al., 2018). If a structure is accessible and inaccessible at the same time, it is called as hybrid structure (Savio et al., 2018). Furthermore, if the truss thicknesses of lattice structure are all same, then it is called homogeneous. If they are different from each other in terms of thickness, it is said to be heterogeneous and if they are changing according to the length of lattice, then it is called gradient cell cellular material (Savio et al., 2018).

2.3.1 Strut-based lattice structures

Body-centered cubic and face-centered cubic are the best known strut-based lattice structures. Some other forms exist as well; for example, body-centered cubic with z struts and face-centered cubic with z struts. Octet truss and diamond cubic topologies also belong to strut-based lattice structure types (Maconachie et al., 2019). In Figure 2.3, strut-based lattice structure shapes are shown.

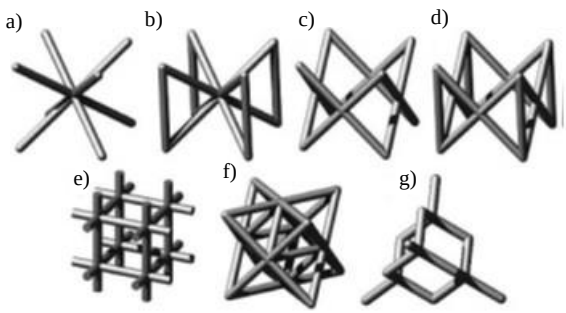

Figure 2.3. Strut-based structures: a) BCC, b) BCCZ, c) FCC, d) FCCZ, e) Cubic, f) Octet-truss, g) Diamond (Maconachie et al., 2019)

These strut-based cell topologies are chosen because of their simplicity of design, and they are obtained through topological optimization processes. Strut-based topologies can be determined by using Maxwell number, M, which is dependent on the number of struts, s, and nodes, n as seen in Equation 2.1 (Maconachie et al., 2019).

$$M = s - 3n + 6 \tag{2.1}$$

There are two conditions. If M<0 means that there are fewer struts than nodes, this leads to the occurrence of excessive moments on struts and these types of structures are defined as bending-dominated. If M>0 means that there are more struts than nodes, struts receive axial tension or compression loads and those can be defined as stretching-dominated. According to this rule, stretch-dominant lattices are stiff in line with their mass and bending-dominated structures are more deformable than stretch-dominant lattice structures.

2.3.2 Triply periodic minimal surface lattice structures

Schoen gyroid, Schwartz diamond, and Neovius are included in triply periodic minimal surface lattice structures. These topologies are created by using the mathematical formula which defines the $U = 0$ iso-surface boundary between solid and void sections. In Figure 2.4, triply periodic minimal surface lattice structures are shown.

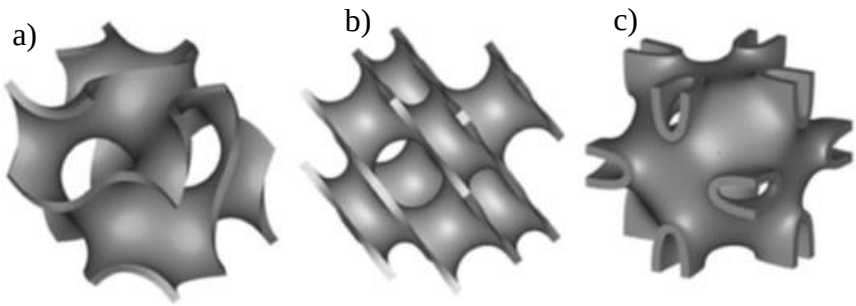

Figure 2.4. Triply periodic minimal surface unit cells: a) Scheon gyroid, b) Schwarz diamond and c) Neovius (Maconachie et al., 2019)

Relative density and periodicity are two important parameters for mechanical properties. TPMS lattice structures are more useful than strut-based structures in terms of manufacturing.

2.3.3 Shell lattice structures

AM is capable of manufacturing cellular structures whose unit cells are plates rather than struts. Those lattice structures can also be defined as TPMS-like, which means their surfaces do not have to be zero mean curvature. Furthermore, closed cell plate-based lattice materials are more elastic than open cell structures even when their densities are similar. Nonetheless, with their remarkably low densities, open cell plate-based structures have certain advantages in terms of manufacturing and stiffness against axial loading conditions.

There are three different types of shell lattice structures, which are single, periodic, and non-intersecting. According to a study carried out by Bonatti and Mohr (2019), triply periodic minimal-surface structures show anisotropic behavior. They also have good energy absorption mechanical properties.

To conclude, a lattice structure is a space filling unit cell, and it can be generated through any axis direction and with no gaps between the cells. Also, different types of lattice structures can be parameterized according to geometry, stochastic, periodic, and gradient dependent topology (Helou & Kara, 2018).

2.3.4 Simple, face-centered and diamond cubic lattice structures

Simple, face-centered, and diamond cubic lattice structures show elastic anisotropic behavior. To decrease anisotropic behavior, simple and face-centered cubic lattices are combined, and they create diamond cubic lattice structure. Octet truss structure shows isotropic elastic behavior at a macro scale, and it is formed by connecting close nodes at FCC structure, which means the truss type is stretching-dominated not bending-dominated (Tancogne-Dejean & Mohr, 2018a). Hollow and solid truss designs do not show the same mechanical properties. Although the second moment of area of solid truss is greater than that of hollow truss, mechanical properties of hollow truss structures are better than those of solid truss structures (Tancogne-Dejean & Mohr, 2018a). Mechanical responses of FCC and body-centered cubic lattice structures are often discussed. However, the effect of anisotropy on the macro scale mechanical responses is not discussed (Tancogne-Dejean & Mohr, 2018a).

Cubic lattice structures can be used as energy absorption materials in defense industry (Dong et al., 2021). Quasi static in plane crushing was studied to show crashing behavior of meta-lattice structures. Initial peak force, mean crashing force efficiency, specific energy absorption and mean crashing force were utilized by creating buckling pattern into the lattice structure (Dong et al., 2021). While producing cubic lattices using the FDM method, the diameter of trusses cannot be exactly the same and this leads to unidentical mechanical properties of cubic lattices. Some finite element methods can predict these differences and calculate elastic modulus of different cubic lattices (Karamooz Ravari et al., 2014). Also, there exist two types of modeling. In the first one, BCC trusses are modeled as beam and in the second model, BCC trusses are modeled as solid meshes. According to research, the beam model cannot simulate the differences and porosities of trusses exactly and the solid mesh model can simulate them better. However, obtained elastic modulus is not significantly different (Karamooz Ravari et al., 2014). In Figure 2.5, solid mesh of unit cell is shown. Moreover, solid mesh is second order, which means all triangles include one more node between two nodes to simulate displacements better.

Figure 2.5. Solid mesh of a unit cell (Zhou et al., 2021)

Moreover, post buckling behavior of simple, face-centered, and body centered cubic lattices are simulated by using the finite element method (Derveni et al., 2022). This study involves three anisotropic structures, which are simple, face-centered, and body-centered cubic lattices, and two isotropic structures, one of which is a combination of simple and body-centered cubic lattices and the other a combination of simple and face-centered cubic lattices. According to a study, a decrease in the thickness of plates or trusses results in an increase in the probability of buckling behavior and post buckling is observed (Derveni et al., 2022). Deformation and energy absorption characteristics change in relation to the manufacturing direction of cubic lattices (Sun et al., 2021b). Octet cell and bending-dominated rhombic dodecahedron (RD) are combined and manufactured with the FDM method. Compression tests are done in their manufacturing direction and their transverse direction. According to research, manufacturing direction is stiffer than transverse direction and their hybrid forms have higher energy absorption coefficients (Sun et al., 2021b).

Furthermore, rather than simple, face-centered, and diamond cubic lattice structures different unit cell geometries can be used for different design purposes. According to a study by Kaur et al. (2017), auxetic materials have negative Poisson's ratio capabilities which enable lattice structures to carry more load capacity and stretching-dominated lattice structures have higher initial yield strength value than bending-dominated lattice structures, which enables stretching-dominated lattice

structures to have more load capacity than bending-dominated lattice structures. In their study, octet truss structures displayed stretching-dominated deformation.

Moreover, although arrangement of octahedral structures does not have the same arrangement with face-centered structures, they can have either bending-dominated or stretching-dominated behavior (Kaur et al., 2017). To predict deformations and failure modes, the finite element model, in which lattice structures have solid mesh, is used. Young's modulus, Poisson's ratio, and density of PLA are entered into the finite element program. Moreover, the analysis method is static and bottom surface of the lattice structures are fixed and upper surfaces of lattice structure are free to move. The finite element analysis method is done to simulate the elastic behavior of lattice structures in linear range. Lattice structures are assumed to be isotropic, which means the material has the same property in all directions x, y and z (Kaur et al., 2017). In Figure 2.6, stress distribution at the intersection point is significantly higher than it is at the other locations of truss.

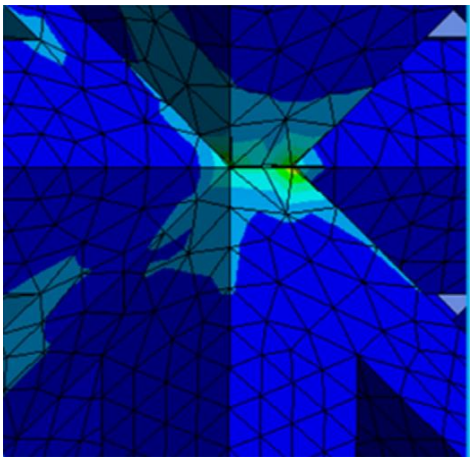

Figure 2.6. Intersection points of octahedral truss structure (Kaur et al., 2017)

According to the finite element analysis and tests, stress is concentrated on the intersection nodes and failures begin at these points (Kaur et al., 2017). In addition, cellular structures can be used for energy absorption purposes. Also, those structures can be classified into two groups as stretching-dominated and bending-dominated. In Figure 2.7, the differences between bending-dominated and stretching-dominated truss structures are shown.

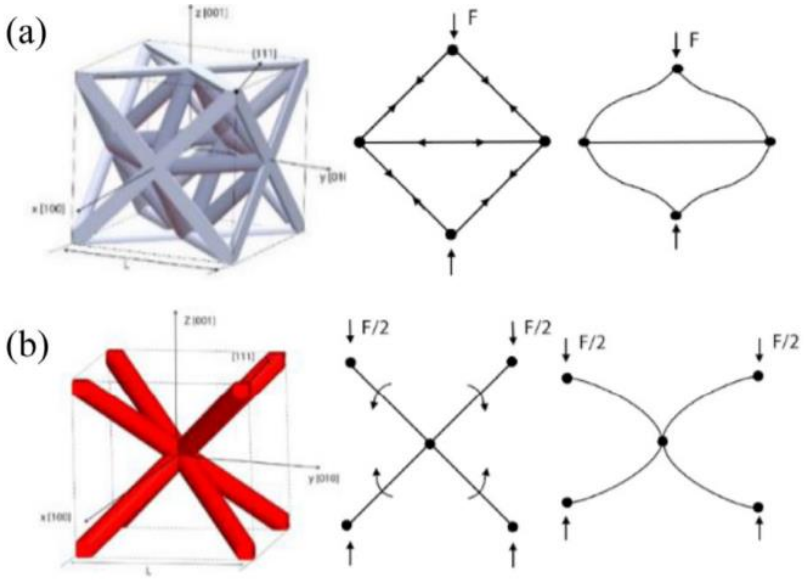

Figure 2.7. Displacement behaviors of stretching-dominated and bending-dominated trusses: a) stretching-dominated displacement behavior of octet truss, b) bending-dominated displacement behavior of BCC (Sun et al., 2021a)

According to Figure 2.7, stretching-dominated and bending-dominated lattice structures are different from each other in terms of displacement behavior. Moreover, relative density and elastic modulus have the linear relationship and FCC is one of them (Sun et al., 2021a). According to research, octet truss shows good energy absorption capabilities because of its deformation mechanism, which is stretching-dominated (Sun et al., 2021a). Bending-dominated structures are BCC, Rhombic Dodecahedron (RD) and Diamond. According to research, elastic modulus of a BCC lattice is lower than FCC lattice though it has the same strut aspect ratio. However, after yielding point, BCC lattice has an advantage for energy absorption condition (Sun et al., 2021a). Amount of energy absorption is calculated from under the area of stress strain curve at compression loading condition. If stress fluctuations were to be decreased, the amount of absorbed energy could increase and unit cell of lattice structure could be modified to increase energy absorption (Sun et al., 2021a). To compare the stretching-dominated lattice structure such as FCC with bending-dominated lattice structure and Diamond which have the same relative density, bending-dominated lattices can carry more load since they can absorb more energy under compressive loading condition (Sun et al., 2021a). Bending-dominated lattice structures are important for energy absorption purposes owing to their stable and

continuous post-yield stress plateau (Sun et al., 2021a). On the other hand, their elastic modulus and initial yield strength points are lower than stretching-dominated lattice structures since their deformation mechanisms tend to deform easily under compression loading.

Moreover, stretching-dominated and bending-dominated lattice structures can be combined to create hybrid structures that have high stiffness and high energy absorption capabilities (Sun et al., 2021a). Mechanical characterization of sandwich panels which consist of 3D printed lattice structures was performed to evaluate shear and bending strength values (Azzouz et al., 2019). Light-weight, high energy absorption coefficient and good stiffness values in compression and bending behavior are the main advantages of sandwich panels.

Sandwich panels consist of two sheets which are located at the upper and lower sections of a core structure. Core structure is useful for compression loading condition, and upper, lower and core structure together are useful for three-point bending behavior. Core structure can be produced with the FDM method, and its shape can be of various lattice structure types such as BCC (Azzouz et al., 2019). In this research, core, upper and lower structures are produced from PLA material using the FDM method (Azzouz et al., 2019). Top and bottom layer of sandwich structure type is non-stochastic and mechanical tests are done to achieve mechanical behavior of in plane and out of plane, core shear and sandwich flexural properties (Azzouz et al., 2019). Traditional honeycomb core structures are well known as good load carriers for compression load cases, but Kagome truss core structures can carry more load than traditional honeycomb structures (Azzouz et al., 2019). A study was conducted by Moeini et al. (2022) to predict the mechanical behavior of the honeycomb structure produced by FDM under compression loading condition. In the study, two different Finite Element (FE) methods were used. The first one was based on beam theory, which uses explicit FE models, and the cell geometry was 3D meshed. The second one was based on 2D mesh and the mechanical properties of cell geometry were found through numerical optimization. It was concluded that cell geometries with 3D mesh yield closer approximation results than those with 2D mesh.

Mechanical behavior of cubic lattices is generally tested under uniaxial compression loading condition; however, multiaxial loading condition is not performed and according to research, multiaxial loading condition and uniaxial loading condition have different mechanical properties. To understand the difference between loading direction, mathematical continuum equations are created (Molavitabrizi et al., 2022).

2.3.5 Additive manufacturing of lattice structures

Lattice structures can be manufactured by either traditional methods such as waterjet cutting, weaving, and braising or AM methods like SLS, SLM and EBM. In traditional methods, there are so many manufacturing steps, but the AM method simplifies those manufacturing steps. There are mainly seven different manufacturing types in AM, which are binder jetting, directed energy absorption, material extrusion, material jetting, powder bed fusion, sheet lamination and vat photopolymerization. The AM method utilizes less material compared to traditional manufacturing methods. For example, the FDM method uses a filament which comes from the nozzle and which is layered on top of each other until the final geometry of the lattice structure is reached. The vat photopolymerization method uses the ultraviolet light to cure photopolymer or other material to produce a lattice structure. To produce lattice structures, AM methods use materials less than the traditional manufacturing methods do (Helou & Kara, 2018). The AM processes are more preferable than traditional manufacturing processes when producing lattice structures since they use materials according to the mechanical design of lattices by directly layering the material through the design and they do not use the disposal material method.

There are two different manufacturing methods utilized to produce lattice structures, which are powder bed fusion technologies of SLS and SLM. Both SLM and SLS use materials such as bronze, steel, titanium, and aluminum (Helou & Kara, 2018). Lattice structures produced by plastics and ceramics can only be produced by the SLS method. Both are utilized to create different types of lattice structures. The SLS process uses atomized powders—physically very small particles of material—and these are sintered through the heat produced by laser. The porosity of the lattice

structures can also be controlled precisely. In this process, material particles are bonded together to form the lattice structure. Voids and inaccuracies are the disadvantages of the SLS process while the SLM process produces homogeneous parts by heating the material until the melting point. However, this process can only be utilized for non-alloy metals. EBM is another AM method for manufacturing lattice structures. EBM is faster than other AM methods to create lattices, but its surface quality is lower than others. The EBM process is almost like SLS and SLM processes, but instead of utilizing a laser, it utilizes an electron beam as a heat source under vacuum condition. There is a material limitation in EBM, and it can only be utilized in metals.

Furthermore, the sheet lamination, material jetting, binder jetting, and directed energy absorption AM methods are not preferred in producing lattice structures. There are some difficulties in producing lattice structures. One of them is that lattices larger than 10 cm cannot be effectively produced by traditional or AM methods since manual processes are required for larger scales.

Another issue is that support structures are needed to complete larger scale lattice structures because manufacturability is getting harder with increasing scale. The SLS process is capable of manufacturing parts without support structures for plastic materials. In order to define a lattice structure, the unit cell should be designed according to the method of generation and inherent properties.

Lattice structures are separated into two fields as manually generated and mathematically generated. Manually generated lattices include beams and truss structures while mathematically generated lattices are created by algorithms. Mathematically generated lattices do not require any post processes to connect the structures. Furthermore, assembly or post-production treatment is always necessary to produce lattice structures with traditional manufacturing methods. Also, hollow truss shapes can be produced by using SLS and SLM manufacturing methods.

Cubic lattices that are produced by AM are used for orthopedic applications. Porous scaffolds can be designed and produced with AM methods, and they can be used to heal damaged bones. Porous scaffolds help to increase proliferation of cells and osseointegration of bone tissues (Agarwal & Gupta, 2017). Implants are generally

used to heal broken bones and the aim is to increase bone growth. However, they may not easily withstand stress shielding effect and as a result fail. In order to resist the stress shielding effect, low dense scaffolds should be manufactured to provide smooth fluid flow and mechanical stability (Agarwal & Gupta, 2017). According to research, open porous space contributes to osseointegration and cell growth (Agarwal & Gupta, 2017). Moreover, porosity can be arranged easily by changing the design of strut. For example, increasing the porosity of scaffolds is beneficial for bone structure; however, increasing porosity causes structural instability (Agarwal & Gupta, 2017). To estimate the mechanical behavior of scaffolds, finite element analysis methods are used to reduce cost and time. To manufacture open cell porous scaffolds, metal-based AM technologies, which are selective laser melting, direct laser deposition, electron beam melting, and selective laser sintering, are used (Agarwal & Gupta, 2017).

DFAM is another concept related to additive manufacturing methods, and it refers to the prediction of geometries, material compositions and sizes of microstructures to optimize the manufacturing process of products. There are mainly three different DFAM methodologies, which are determining the surface position of the desired design, optimizing—which can be numerical and functional—and drawing manufacturing steps according to the optimization technique of the design.

Ti-6Al-4V is a material now used for biomedical applications. Before the AM technology, however, titanium and titanium alloys were used for orthopedic applications and stress shielding problems occurred. A stress shielding problem occurs when the stiffness of human bone and that of titanium are not matched with each other. To overcome this problem, porous structures can be manufactured with AM technology (Sallica-Leva et al., 2016). Ti-6Al-4V alloy is generally used for aerospace applications due to its high strength and low weight ratio and it is also used for biomedical applications due to its biocompatibility. Heat treatment methods are effective in increasing the mechanical properties of Ti-6Al-4V titanium alloy (Sallica-Leva et al., 2016).

Lattice structures can be manufactured for different engineering applications with the aid of AM methods. One of them is to produce energy absorption materials for the

desired range of impact. In their research, Ozdemir et al. (2016) focused on the characteristics of dynamic behavior of cubic lattices under different impact loading conditions. While testing the impact analysis of lattices, Hopkinson pressure bar tests were done. According to the test results, cubic lattices can distribute the impact of loading to decrease the peak impact stress on the structure (Ozdemir et al., 2016). It was also revealed that, simple and diamond cubic lattice structures are able to withstand impact loads more efficiently than other lattice types.

2.3.6 Design and optimization of lattice structures

Lattice structures can be classified into two groups as uniform lattice structures and non-uniform lattice structures. The design and optimization of uniform lattice structures can be separated into three groups as unit cell structure design, mathematical algorithm, and unit cell topology optimization (Pan et al., 2020). The formation of unit cells in the lattice structure determines the category of lattice structures. Different unit cells have different characteristics based on their lattice structure shapes.

Mainly, there are three ways to describe optimization methods for lattice structures, and they are uniform lattice structures formed based on the design of unit cell shape, uniform lattice structures formed based on mathematical algorithm, and uniform lattice structures formed based on the optimization of unit cell topology (Pan et al., 2020). Moreover, closed-walled shell structures are more optimal than lattice structures, but lattice structures are more stable and easier to manufacture than others. Lattice structures are generally aligned with regular grid position and the method of aligning grids according to principal stresses are a useful way to optimize lattice structures (Wu et al., 2021). This principle can be applied to 2D planes and curved surfaces. The method aims to maximize the stiffness matrix of lattice structure according to the static load. Topology optimization is an important method for 3D mechanical parts. Topology optimization arranges mechanical shape and materials according to constraints. The homogenization method determines the distribution of square unit cells with variable rectangular holes. The Homogenization-based optimization method was the first optimization method for

lattice structures, and it was introduced by Bendsoe and Kikuchi (Hoang et al., 2020). Among the different types of optimization methods, the homogenization method is the most useful one because the microstructure of lattices can be shaped according to its effective properties in the homogenization-based approach. During the homogenization-based optimization process, first a draft lattice is created in different densities and then this model is used for the steps of the optimization process, which helps computers to decrease calculation time. A mapping function related to optimized orientation is crucial to project the homogenized design (Fernandes & Tamijani, 2021). Optimization starts with a coarse mesh and then the optimized design is projected onto a fine mesh with the aid of mapping function and the lattice structure is created with optimized design density. If stress constraints are not determined as part of the optimization process, the method could not create lightweight periodic lattice structure (Fernandes & Tamijani, 2021). The utilization of stress states changes the topology and morphology of lattice structures.

There are mainly three difficulties in stress constraints. These are stress singularities at zero density, the large number of local stress constraints and the local micro stresses (Fernandes & Tamijani, 2021). Moreover, stress singularities and a large number of local stress constraints can exist in macro and micro structural optimization. Usually, macrostructural optimization by taking into account microstructural constraints is not useful. There are two ways to put microstructural constraints in the macrostructural optimization method. The first one is finding the effective allowable stresses and the second one is detailing the homogenized stress (Fernandes & Tamijani, 2021). Compliance-based lattice structure topology and morphology optimization is another optimization method, and this method uses load paths and load flows as intermediate variables. Moreover, modified Hill yield criteria can be used as stress constraints in lattice structures.

Topology optimization is a more productive method than others. An efficient amount of material is used to carry the same load capacity with traditional non-optimized structural parts. There are different types of topology optimization methods in literature. Simplified isotropic material with penalization (SIMP), level-set and evolutionary structural optimization (ESO) are some of the widely known topology optimization methods (Hoang et al., 2020). Traditional topology optimization

methods use elements or nodes as design variables to fit different constraints. SIMP, ESO and level-set topology optimization methods use element density function which is implicitly given to converge the problem. Also, SIMP is the most useful method since implementation of variables and control of the size of structure is easier than others. Recent topology optimization methods have explicit solutions rather than implicit ones. The use of multi-layer materials, fewer design variables, modeling simplicity and connection with computer aided design programs are advantages of new topology optimization methods.

All those optimization methods aim to calculate effective element density by using geometric components. A lattice structure repeats itself into the unit cell, and the shape of microstructure in lattice has a strong effect on mechanical properties. Because of the non-uniform properties of lattice structures, optimization methods focus on microstructural properties rather than macrostructural ones. Multiscale topology optimization can be used for two-phase microstructures, coated structures with orthotropic infill and functionally graded materials (Hoang et al., 2020), while the concurrent optimization method is used together with microstructure and macrostructure optimization process.

There are different ways to design cubic lattice structures. Removing material from trusses according to the load path is one of them. This process returns the bending-dominated structure to stretching-behavior structure or vice versa. To illustrate, a simple cubic lattice structure can be both stretching-dominated and bending-dominated structure and it is related with applied load on cubic lattice (Tancogne-Dejean & Mohr, 2018b). Relative density equations can be obtained from the Equation 2.2,

$$\rho^* = C_1(\frac{R_o}{L})^2 - C_2(\frac{R_o}{L})^3 \tag{2.2}$$

In Equation 2.2, R_o is the outer diameter of beam structure and L is the height of the beam (Tancogne-Dejean & Mohr, 2018b). C_1 and C_2 are the constants and can be determined from lattice cell topologies. If the beam is hollow, then Equation 2.3 will be used to find the relative density of the lattice structure,

$$\rho^* = C_1\left(\frac{R_o}{L}\right)^2\left(1-\left(\frac{R_i}{R_o}\right)^2\right) - C_2\left(\frac{R_i}{L}\right)^3\left(1-\left(\frac{R_i}{R_o}\right)^3\right) \tag{2.3}$$

In Equation 2.3, R_i is the inner diameter of beam structure.

2.3.7 Analytical analysis of lattice structures

Cellular material structures can be analytically analyzed in two different ways. The first one is Ashby-Gibson model (Peng et al., 2020). The most important property is ρ^*/ρ for cellular material structures. Face connectivity, size and shape are also useful to characterize mechanical properties of cellular material structure. However, those mechanical properties are not taken into account for this analytical model (Peng et al., 2020). In Figure 2.8, Ashby-Gibson model and its mechanical behaviors can be seen.

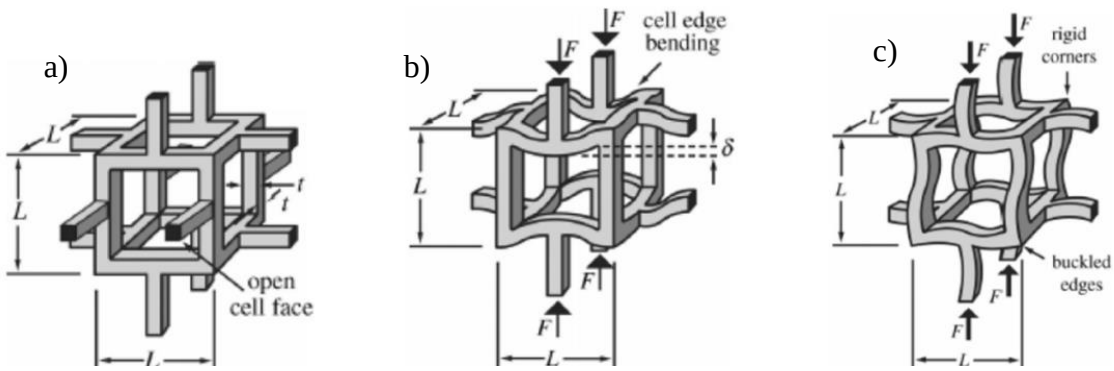

Figure 2.8. a) Ashby-Gibson model, b) Bending behavior of Ashby-Gibson model, c) Buckling behavior of Ashby-Gibson model (Peng et al., 2020)

According to the assumptions, a mathematical equation is found, and it shows the relation between Young's modulus of cellular material structure and its density ratio.

$$\frac{E^*}{E} = C_1\left(\frac{\rho^*}{\rho_s}\right) \tag{2.4}$$

In Equation 2.4, E^* is the elastic modulus of cellular material structure, E is the elastic modulus of material, ρ^* is the density of cellular material structure and ρ_s is the density of solid material and C1 is nearly one according to experimental mechanical tests (Peng et al., 2020). Furthermore, according to this model, inhomogeneous material property, mechanical torsion effects in the corners and arbitrary loading condition are neglected (Peng et al., 2020).

The second analytical analysis method for cellular material structures is the Zhu method. Zhu realized that mechanical buckling behavior is observed during uniaxial compression loading condition (Peng et al., 2020). According to the Zhu model, bending, stretching, and twisting of trusses are covered and is shown in Equation 2.5,

$$\frac{E^*}{E_s} = 2/3C_2(\frac{\rho^*}{\rho_s})^2(1 + C_2(\frac{\rho^*}{\rho_s}))^{-1} \tag{2.5}$$

In Equation 2.5, E^* is the elastic modulus of cellular material structure, E_s is the elastic modulus of solid material, ρ^* is the density of cellular material structure, ρ_s is the density of solid material. $C_2 = \frac{8\sqrt{2}I}{A^2}$, where I is the moment of inertia and A is the second moment area (Peng et al., 2020).

2.3.8 Finite element analysis of cubic lattices

To understand the mechanical behavior of cubic lattices, finite element analysis is done. Moreover, linear static analysis is useful in predicting the mechanical behavior of cubic lattices. Boundary conditions are given from the bottom of the cubic lattice and distributed load is applied from the upper section of the cubic lattices as if they are compressed in universal axial compression machine (Agarwal & Gupta, 2017).

Generally, cubic lattices are investigated and analyzed under uniaxial loading condition. Multiaxial loading condition can be differentiated from uniaxial loading condition through their matrix form (Molavitabrizi et al., 2022). In Equation 2.6, uniaxial, biaxial, and multiaxial forms can be seen,

$$\text{Uniaxial: } \begin{bmatrix} \in_{xx} & 0 & 0 \\ 0 & 0 & 0 \\ 0 & 0 & 0 \end{bmatrix}$$

$$\text{Biaxial: } \begin{bmatrix} \in_{xx} & 0 & 0 \\ 0 & \in_{yy} & 0 \\ 0 & 0 & 0 \end{bmatrix} \tag{2.6}$$

$$\text{Triaxial: } \begin{bmatrix} \in_{xx} & 0 & 0 \\ 0 & \in_{yy} & 0 \\ 0 & 0 & \in_{zz} \end{bmatrix}$$

CHAPTER 3

3. MATERIALS AND METHODS

3.1 Materials

PLA was used for extrusion and thermoforming applications since it has a high molecular weight, and it shows less fluidity at the molten state. The average molecular weight of PLA is $M_{n(PLA)}$ =74500. Polydispersity index is $\frac{M_w}{M_n}$ = 2, L/D-isomer ratio is 96/4. MFI (190 °C, 2.16 kg) of 6.6 g/10 min (Murariu et al., 2010).

3.1.1 Characterization of PLA with FTIR, XRD and DSC methods

PLA characterization tests were done with Fourier-transform infrared spectroscopy (FTIR), X-Ray Diffraction Analysis (XRD) and Differential Scanning Calorimetry (DSC).

3.1.1.1 Characterization of PLA with FTIR method

The tests were done at METU Central Laboratory with PERKIN ELMER Spectrum 400. The FTIR test was done to obtain infrared spectrum of absorption of a PLA material.

3.1.1.2 Characterization of PLA with XRD method

XRD method was used to characterize the PLA material by using Ultima-IV machine since XRD helps to identify the arrangement of nanoparticles in material. The scan speed of XRD was 1 deg/min and the scan range was from 10 degrees to 90 degrees.

3.1.1.3 Characterization of PLA with DSC method

The DSC test was done to characterize the thermal stability of the PLA material. Between 25°C and 290°C with velocity of 10°C/min the TGA test was conducted for one sample in DSC250 air condition.

3.2 Production of lattice structures by FDM

In this thesis, three different types of cubic lattices (simple cubic, face-centered cubic and diamond cubic lattices) were studied as seen in Table 3.1. Moreover, four different parameters were applied to simple, face-centered and diamond cubic lattice structures, which were with radius, without radius, hollow, and hollow and with radius. They were manufactured by using PLA. The length of the cubic lattices was 40 mm for all types of cubic lattices, while truss diameters were 3.2 mm for all types of cubic lattices and their different parameters. Furthermore, outer diameter of truss was 3.2 mm and inner diameter of truss was 1.6 mm for hollow truss parameters. Radii at the junction point of trusses were 3 mm. In addition, each type of sample was manufactured three times and they were tested mechanically under compression loading condition. Identifications were assigned according to cubic lattice types and their parameters, as shown in Table 3.1. All samples were produced in Raise 3D Pro2 Plus FDM machine. Manufacturing parameters were fixed for all lattice types and their different parameters. In Table 3.2, FDM parameter types and their manufacturing values are shown.

Table 3.1. Identification of lattice types and their explanations

Lattice structures	Notation Identify of Samples	Explanation	# of samples
Simple Cubic	SC-R	Simple cubic lattice with radius parameter	3
	SC-WR	Simple cubic lattice without radius parameter	3
	SC-R-H	Simple cubic lattice with radius and hollow truss parameter	3
	SC-WR-H	Simple cubic lattice without radius and hollow truss parameter	3
Face-centered Cubic	FC-R	Face-centered cubic lattice with radius parameter	3
	FC-WR	Face-centered cubic lattice without radius parameter	3
	FC-R-H	Face-centered cubic lattice with radius and hollow truss parameter	3
	FC-WR-H	Face-centered cubic lattice without radius and hollow truss parameter	3
Diamond Cubic	DC-R	Diamond cubic lattice with radius parameter	3
	DC-WR	Diamond cubic lattice without radius parameter	3
	DC-R-H	Diamond cubic lattice with radius and hollow truss parameter	3
	DC-WR-H	Diamond cubic lattice without radius and hollow truss parameter	3

Table 3.2. FDM parameter types and their manufacturing parameters

FDM parameter types	Manufacturing parameters	Values
Layer	Layer height [mm]	0.15
	First layer height [mm]	0.3
	First layer solid fill pattern type	Lines
	Minimal segment length [mm]	0.012
Extruder	Extrusion width [mm]	0.4
	Retraction speed [mm/s]	40
Infill	Infill density [%]	15
	Infill overlap [mm]	5
	Infill flowrate [%]	100
	Infill pattern type	Grid
Solid Fill	Bottom solid fill layers	5
	Top solid fill layers	5
	Top surface solid fill pattern type	Lines
	Bottom surface solid fill pattern type	Lines
Temperature	Heated bed temperature [°C]	60
	Left extruder [°C]	205
	Right extruder [°C]	205
Speed	Default printing speed [mm/s]	50
	Infill speed [mm/s]	80
	Support speed [mm/s]	50

3.3 Mechanical testing

In this thesis, three different types of cubic lattices (simple cubic, face-centered cubic and diamond cubic lattice structures) were studied. Also, each lattice structure had four different parameters, which were with radius, without radius, hollow, and hollow and with radius. Moreover, twelve cubic lattices were mechanically tested under compression load for one cubic lattice type, and totally thirty-six cubic lattices were tested separately under compression loading condition. Before the test began, weight and displacement values of mechanical test machine were set as zero and then the test started. During mechanical testing, force and displacement values were recorded. Mechanical compression test was done in the speed of 1 mm/min. The end

of test parameter was 50% of the maximum load applied on structure, which means the test ended when 50% of maximum load was observed during testing.

3.4 Finite Element Analysis

To simulate the mechanical behavior of cubic lattices under compression loading condition, the finite element analysis method was used. Altair Hypermesh was used as a pre-processor for modeling cubic lattices and Altair Hyperview was used as a post-processor to simulate the mechanical behavior of cubic lattices. Nastran was used as a solver for finite element models. One-dimensional elements (Cbar, Cbeam) were used to simulate cubic lattice models. They had the same degree of freedom and Cbeam model did not include warping effects. SOL400 (Implicit Nonlinear Static Analysis) was used as a Nastran solver type.

3.4.1 One dimensional element CBAR

Cbar is used to define a simple beam element for structural analysis methods. Cbar is a one-dimensional element, which means it is used to connect two different nodes having six degrees of freedoms. Truss elements in cubic lattices are modeled as Cbar. Furthermore, grid point A and grid point B should be determined before the creation of Cbar. Grid point A can be [0 0 0] in global axis and grid point can be [40 0 0] in global axis. After the determination of grid points, element orientation vectors should be selected to create section of truss elements. If the truss element is along the x global axis, orientation vector should be selected as < 0 1 0 > or <0 0 1> to create truss section. Both vectors can be selected since truss section is circular. If truss element is along the global y axis, orientation vector should be <1 0 0 > or < 0 0 1> to create truss section. In this study, simple cubic, face-centered cubic, and diamond cubic trusses were prepared in pre-process according to those structural element properties. In Figure 3.1, solid truss section and hollow truss section are shown.

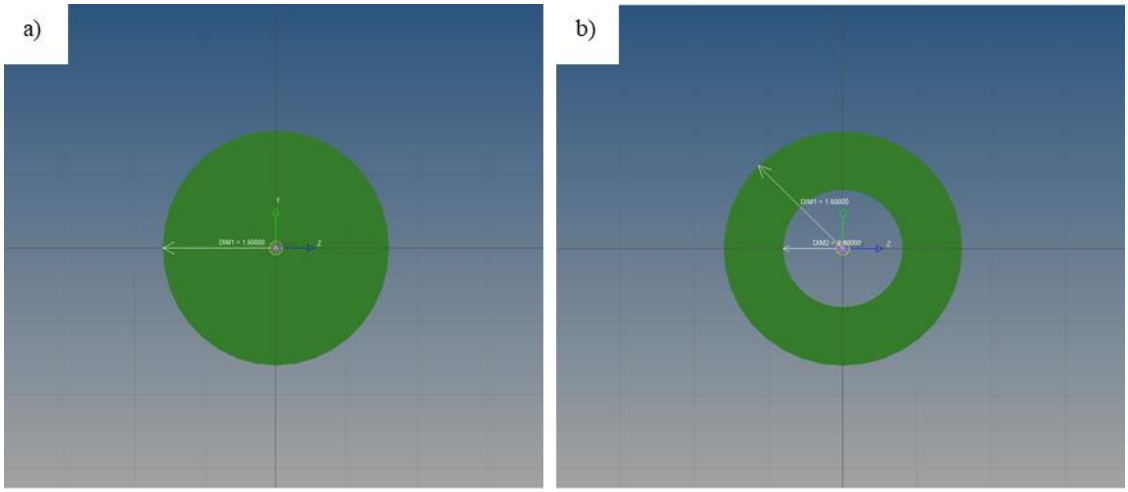

Figure 3.1. a) Solid truss section, b) Hollow truss section

In Table 3.3, the trusses used in simple, face-centered and diamond cubic lattices area, moments of inertia, and centroidal and principal axes values are shown.

Table 3.3. Analytical calculations of solid and hollow trusses

Solid Truss	Hollow Truss
Area = 8.0425 mm^2	Area = 6.0319 mm^2
Centroid :	Centroid :
Local	Local
Yc = 0.0000	Yc = 0.0000
Zc = 0.0000	Zc = 0.0000
Moments Of Inertia :	Moments Of Inertia :
Local	Local
IY = 5.1472 mm^4	IY = 4.8255 mm^4
IZ = 5.1472 mm^4	IZ = 4.8255 mm^4
IYZ = 0.0000	IYZ = 0.0000
Centroidal	Centroidal
IY = 5.1472 mm^4	IY = 4.8255 mm^4
IZ = 5.1472 mm^4	IZ = 4.8255 mm^4
Iyz = 0.0000	Iyz = 0.0000
Principal	Principal
Iv = 5.1472	Iv = 4.8255
Iw = 5.1472	Iw = 4.8255
Angle = 0.0000	Angle = 0.0000
Polar = 10.2944	Polar = 9.6510
Radius of Gyration = 0.8000	Radius of Gyration = 0.8944
Torsional Constant = 10.2944	Torsional Constant = 9.6510
Warping Constant = 0.0000	Warping Constant = 0.0000
Shear center :	Shear center :
Local	Local
Ys = 0.0000	Ys = 0.0000
Zs = 0.0000	Zs = 0.0000
Principal	Principal
Vs = 0.0000	Vs = 0.0000
Ws = 0.0000	Ws = 0.0000
Shear factors	Shear factors
Ky = 0.9000	Ky = 0.5000
Kz = 0.9000	Kz = 0.5000
Elastic Sect Mod :	Elastic Sect Mod :
Centroidal	Centroidal
Sy = 3.2170	Sy = 3.0159
Sz = 3.2170	Sz = 3.0159
Principal	Principal
Sv = 3.2170	Sv = 3.0159
Sw = 3.2170	Sw = 3.0159
Max Coord Ext :	Max Coord Ext :
Centroidal	Centroidal
y = 1.6000	y = 1.2000
z = 1.6000	z = 1.2000
Principal	Principal
v = 1.6000	v = 1.2000
w = 1.6000	w = 1.2000
Elastic Tors Mod = 6.4340	Elastic Tors Mod = 7.2382

3.4.2 Modeling of cubic lattices with CBAR structural element method

In Figure 3.2, Simple cubic lattice, face-centered cubic lattice and diamond cubic lattice structures modeled by using Cbar element are shown. The bottom of each cubic lattice is fixed at six degrees of freedoms and force is applied from upper section of the lattices. Force is applied equally on all nodes at the upper section of lattices by using rigid body element (RBE2). RBE2 element helps to distribute the load which is applied through global z axis to the upper section of cubic lattices.

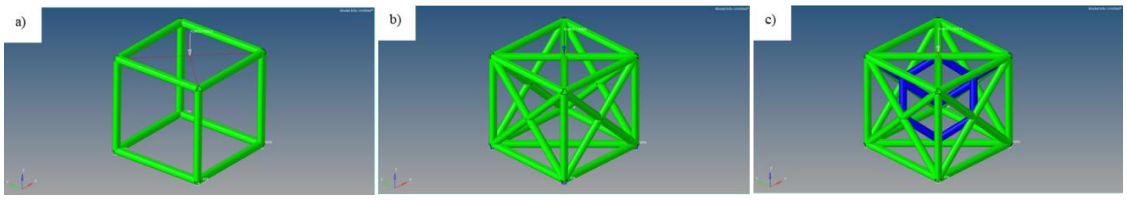

Figure 3.2. a) Simple cubic lattice, b) Face-centered cubic lattice, c) Diamond cubic lattice

CHAPTER 4

4. RESULTS & DISCUSSION

4.1 Characterization of PLA with FTIR, XRD and TGA methods

4.1.1 Characterization of PLA with FTIR method

In Figure 4.1, PLA is characterized with FTIR method. Peak values of spectra can be seen. The first vibration of PLA is nearly 2988 and 2954 cm^{-1}, and this vibration refers to C-H bond. Furthermore, considerable peak value is seen at 1750 cm^{-1} and 1182 cm^{-1}, and those values show the C=O and C-O-C bond, respectively. Moreover, O-H band of PLA is changing according to the wave number, and at the 1650 cm^{-1} wave number, O-H band is observed. There is a small vibration peak since it occurs bending of the unresolved hydroxyl group of water and it carried with cellulose (Mofokeng et al., 2012).

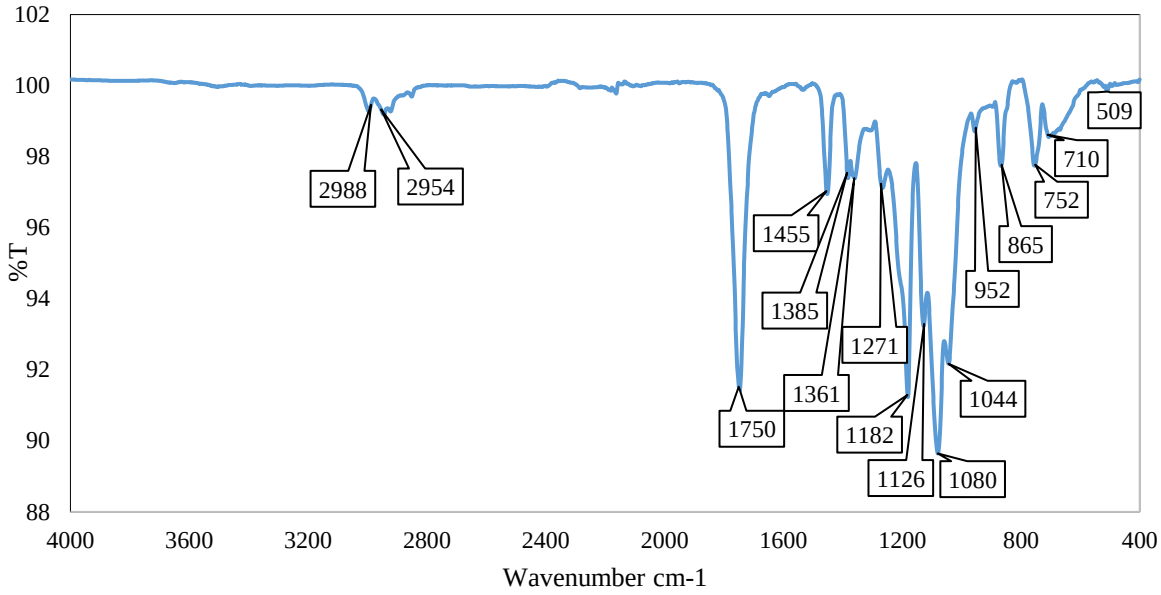

Figure 4.1. FTIR result of PLA

4.1.2 Characterization of PLA with XRD method

PLA structure was analyzed with XRD method to detect pure PLA. In Figure 4.2, XRD pattern can be seen. According to the figure, maximum intensity is observed at nearly 2Θ = 16°. This shows the PLA had no polymorphic crystalline transition.

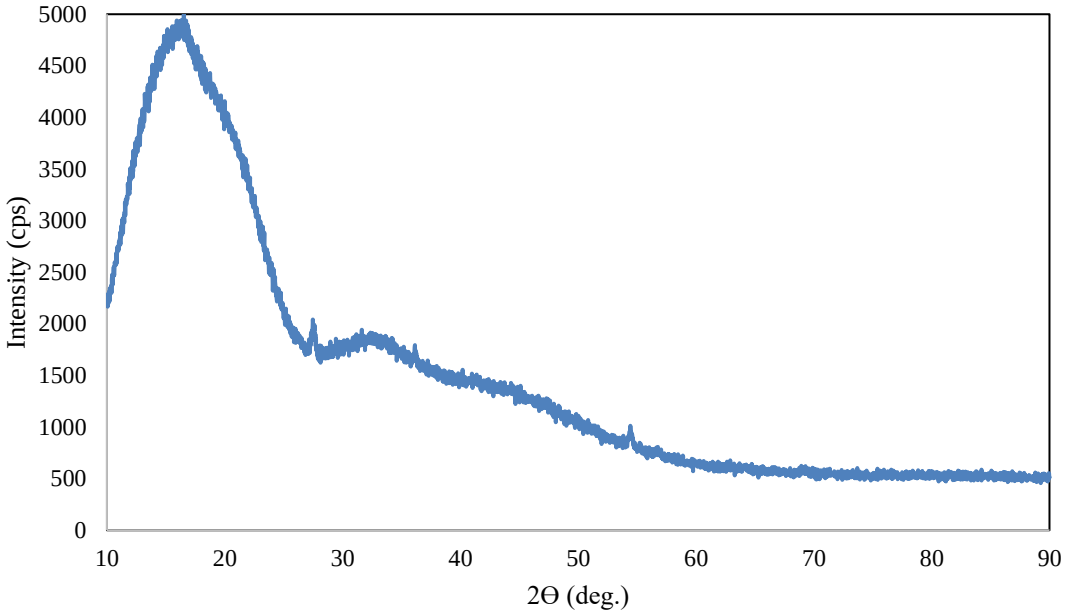

Figure 4.2. XRD result of PLA

4.1.3 Characterization of PLA with the DSC method

The Differential Scanning Calorimetry (DSC) results of PLA are shown in Figure 4.3. The glass transition, cold crystallization, and melting point of sample can also be seen. PLA's DSC graph shows glass transition, crystallization exotherm and melting endotherm peaks. Glass transition temperature of PLA is 151.68 °C from first heating.

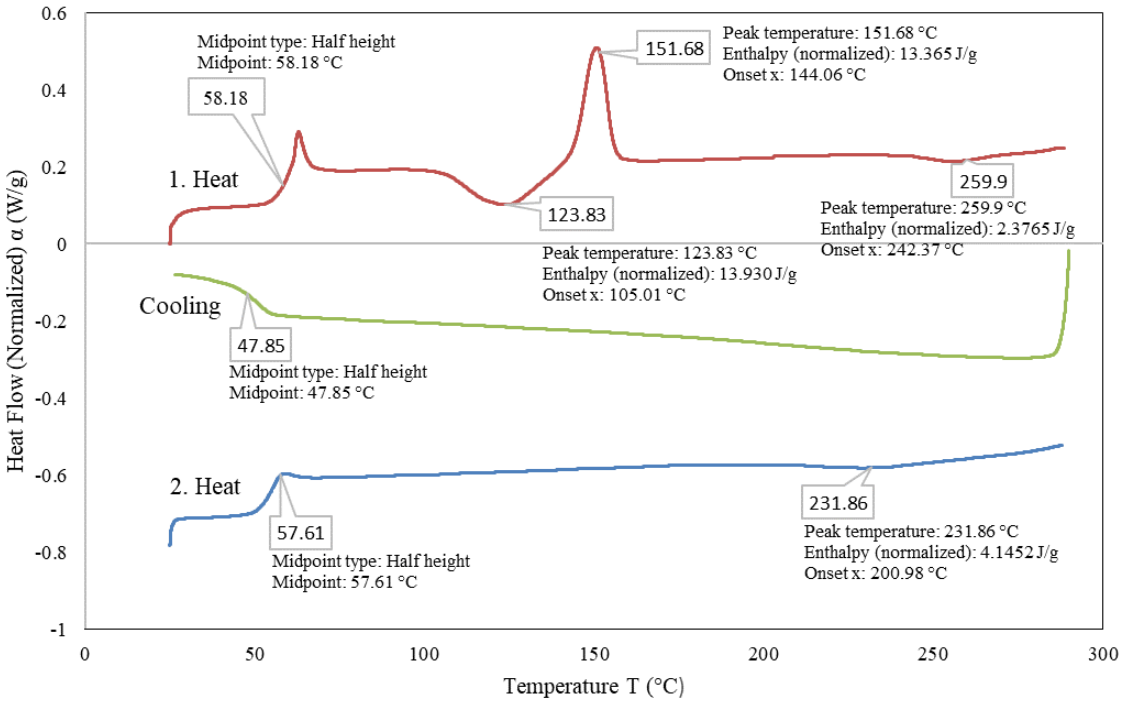

Figure 4.3. DSC result of PLA

4.2 Mechanical testing of simple cubic lattices

In Figure 4.4, compression test results of simple cubic lattices according to the manufacturing direction are given. The modulus of elasticity is nearly the same for all samples and different parameters. Ultimate tensile strengths (UTS) for simple cubic lattices are almost the same for three different samples. Finite element analyses were done for each parameter and stress-strain values of cubic lattices were calculated.

In Figure 4.5, compression test results of simple cubic lattices according to non-manufacturing direction are given. Generally, the UTS points and strain values change in relation to the manufacturing direction and non-manufacturing direction. Also, samples which were tested through non-manufacturing direction showed ductile material properties and manufacturing direction showed brittle material properties. The reason for the difference in material behavior for Non-manufacturing direction is the buckling phenomenon. Under compression loading condition through non-manufacturing direction, trusses were firstly buckled and then could not transfer

load from the upper section to the lower section and finally were broken off. In addition, the samples which were compressed through manufacturing direction were also buckled. However, buckling phenomenon was observed earlier than samples with non-manufacturing direction and they failed quickly when compared to non-manufacturing direction samples.

According to the Ashby-Gibson model, simple cubic lattices can show buckling phenomenon in two different ways (Peng et al., 2017). In this study, in the first one, horizontal trusses were buckled, in the second phenomena vertical trusses were buckled. Furthermore, simple cubic lattice under compressive loading condition was buckled from vertical trusses and then broke off. During the mechanical compression test, buckling phenomenon of trusses was observed in both vertical and horizontal trusses of all the mechanical designs.

In Figure 4.4 and 4.5, there are some differences between each sample in terms of their UTS points and their elastic modulus because there can be manufacturing differences between samples, and this leads to different mechanical properties under compression load. In literature, while producing cellular structures with the FDM method, differences may occur owing to the manufacturing environment and the 3D printing machine used (Karamooz Ravari et al., 2014). Finite element analysis methods cannot simulate the porosities of trusses on simple cubic lattice and this causes differences between finite element model simulation and mechanical compression test.

To simulate the mechanical behavior of cubic lattices under uniaxial compression loading condition, the linear static analysis method can prove useful. Boundary conditions can be given from the bottom section of cubic lattices and load can be applied as distributed load from the upper section of the cubic lattices (Agarwal & Gupta, 2017). Nonlinear material and nonlinear geometrical type of analysis (SOL400) was performed to simulate mechanical compression test of simple cubic lattices. Furthermore, trusses were modeled as 1D element and middle section displacements of trusses could not be observed. To observe buckling phenomenon and middle section displacements of trusses, linear buckling analysis (SOL105) was performed.

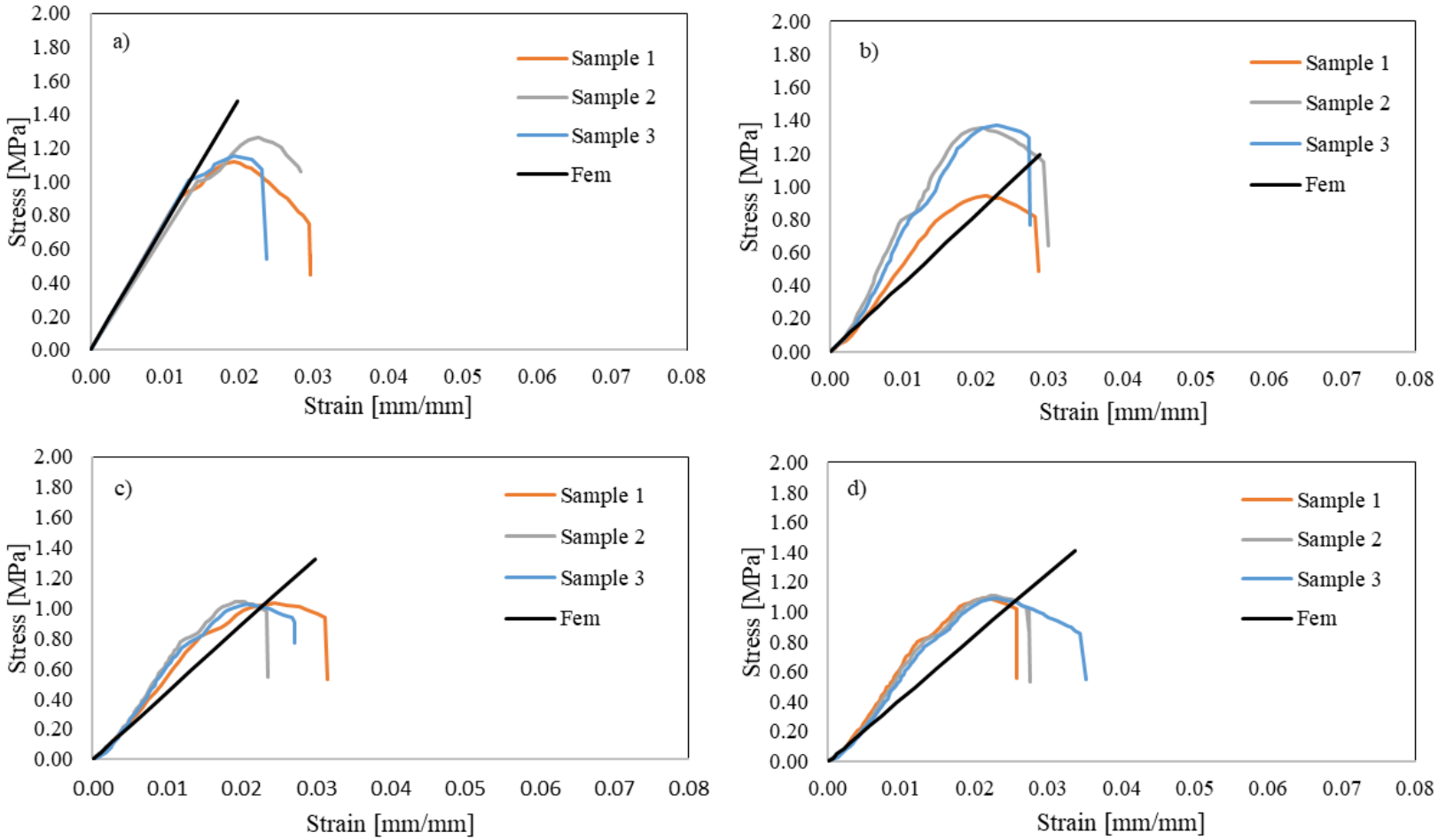

Figure 4.4. Compression test results of a) SC-WR-M, b) SC-R-M, c) SC-WR-H-M, d) SC-R-H-M

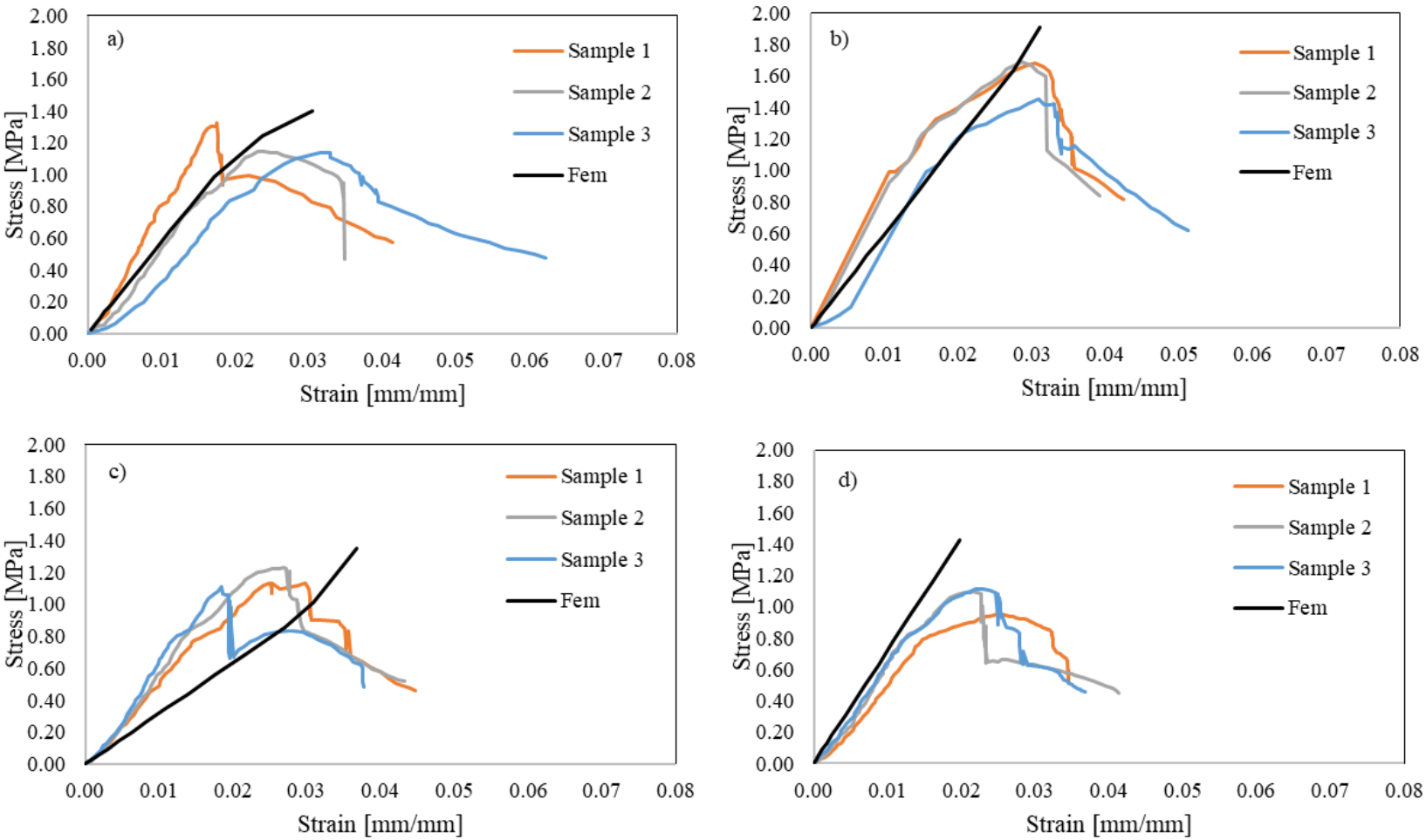

Figure 4.5. Compression test results of a) SC-WR-NM, b) SC-R-NM, c) SC-WR-H-NM, d) SC-R-H-NM

In Table 4.1, simple cubic lattice UTS values and their weight comparison are shown. In this table, reference model is simple cubic lattice without radius parameter and other calculations were done according to values of SC-WR parameter in terms of UTS and weight. Behavior of mechanical properties is different between manufacturing and non-manufacturing direction tests.

Firstly, addition of radius increases stiffness of trusses. The UTS value increased by 13.33% from without radius parameter to radius parameter while weight increased by 8.51%. The UTS value decreased by 8.89% from without radius to hollow truss parameter and weight also decreased by 18.81%. Moreover, when radius was added at the junction points of hollow trusses, the UTS value decreased by 5.19% according to without radius parameter and weight decreased by 10.31% from without radius to radii with hollow trusses parameter. Furthermore, as can be seen from Table 4.1, the addition of radii at the trusses increased the stiffness of simple cubic lattices which were tested through manufacturing direction.

Secondly, the addition of radii at the trusses increased the UTS value from without radius parameter to radius parameter in the mechanical tests related to non-manufacturing direction. Radius increased the UTS value by 40.30% while increasing the weight by 8.51%. Hollow truss decreased the UTS value by 0.75% while decreasing the weight by 18.81%. Hollow truss and radius parameter decreased the UTS value by 2.24%, while decreasing the weight by 10.31%.

Finally, the addition of radii at the trusses increased the UTS value for each parameter and increased the weight, and removing material from the center of trusses decreased the UTS value for manufacturing and non-manufacturing direction of tests.

Table 4.1. Strength and weight reduction rate calculation for simple cubic lattices

Manuf direction	Manufacturing direction of samples				None manufacturing direction of samples			
Type of parameter	WR	R	WR-H	R-H	WR	R	WR-H	R-H
Sigma_UTS [MPa]	1.35	1.53	1.23	1.28	1.34	1.88	1.33	1.31
Weight [g]	3.88	4.21	3.15	3.48	3.88	4.21	3.15	3.48
Strength R, WR-H, R-H vs WR [%]	-	13.33	-8.89	-5.19	-	40.30	-0.75	-2.24
Weight R, WR-H, R-H vs WR [%]	-	8.51	-18.81	-10.31	-	8.51	-18.81	-10.31

In Figure 4.6, the results of simple cubic lattice finite element model in terms of the displacement can be seen. Other parameters for simple cubic lattice were modeled as the same; however, material properties were different for each design parameter. Simple cubic lattice was displaced as 6.70 mm through z direction after uniaxial compressive load.

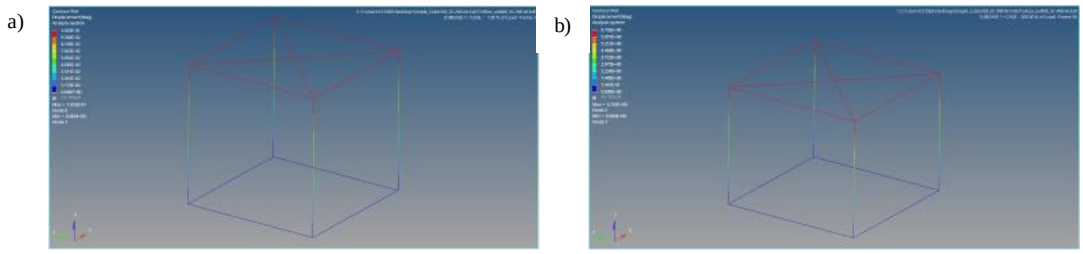

Figure 4.6. a) SC FEM modeling before compression load, b) SC FEM modeling after compression load

In Figure 4.7, before, during and after stages of the mechanical compression test of simple cubic lattice can be seen. The vertical truss structures of simple cubic lattice were buckled and after buckling failure, trusses could not transfer load from the upper section to the lower section and broke off.

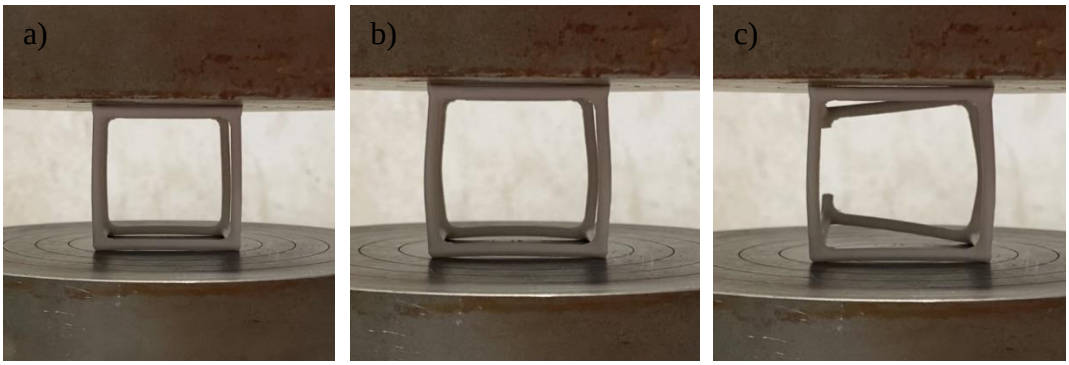

Figure 4.7. a) SC before the test, b) SC during the test, d) SC after the test

In Figure 4.8, the results of buckling analysis are shown. The analysis was done by using SOL105 from Nastran solver. The first eigenvalue is 0.182, which means simple cubic lattice structure was buckled 18% of quasi static compression load. After that phenomena vertical trusses cannot transfer load from upper section to lower section of simple cubic lattice.

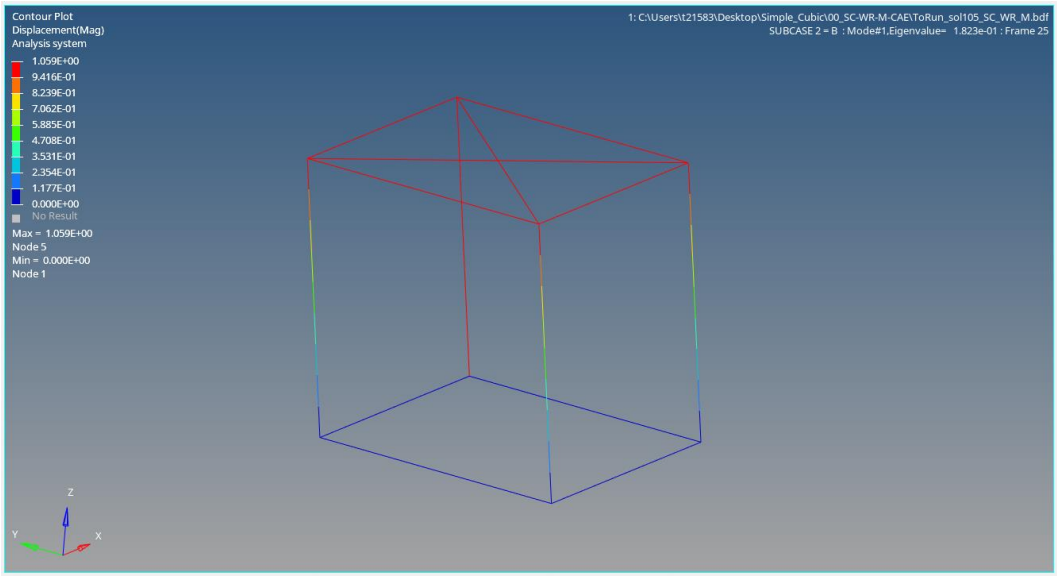

Figure 4.8. SC first eigenvalue mode

In Figure 4.9, the second eigenvalue of simple cubic lattice under compressive load is shown. The eigenvalue is 0.182, which means simple cubic lattice was buckled under 18% of quasi static load.

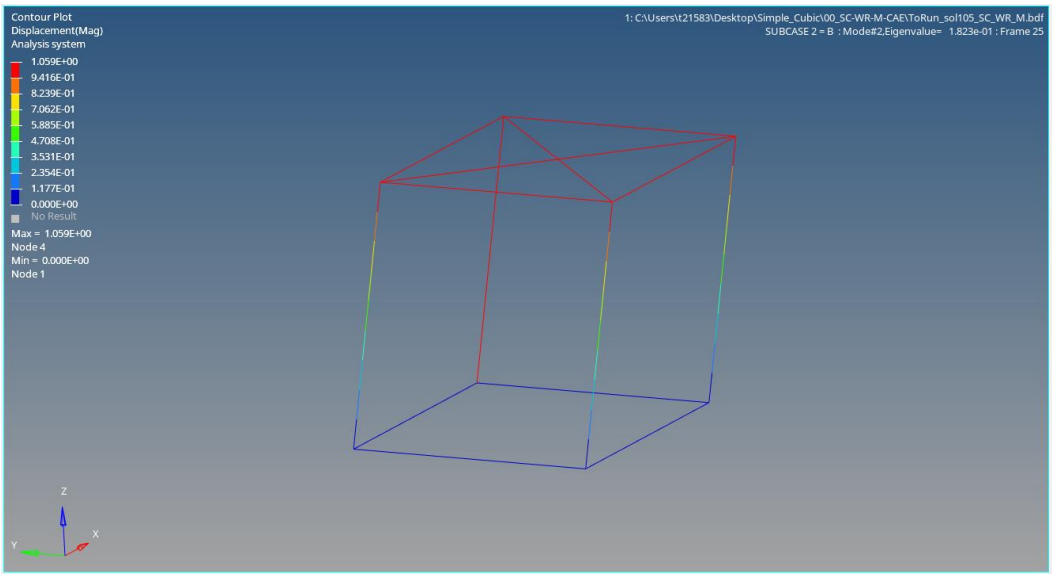

Figure 4.9. SC second eigenvalue mode

As seen in Figure 4.10, failure modes of simple cubic lattices according to manufacturing direction changes and the difference is apparent. Simple cubic lattices which are compressed through the manufacturing direction behave brittle and one of the trusses generally breaks off, while they behave ductile when compressed through the non-manufacturing direction.

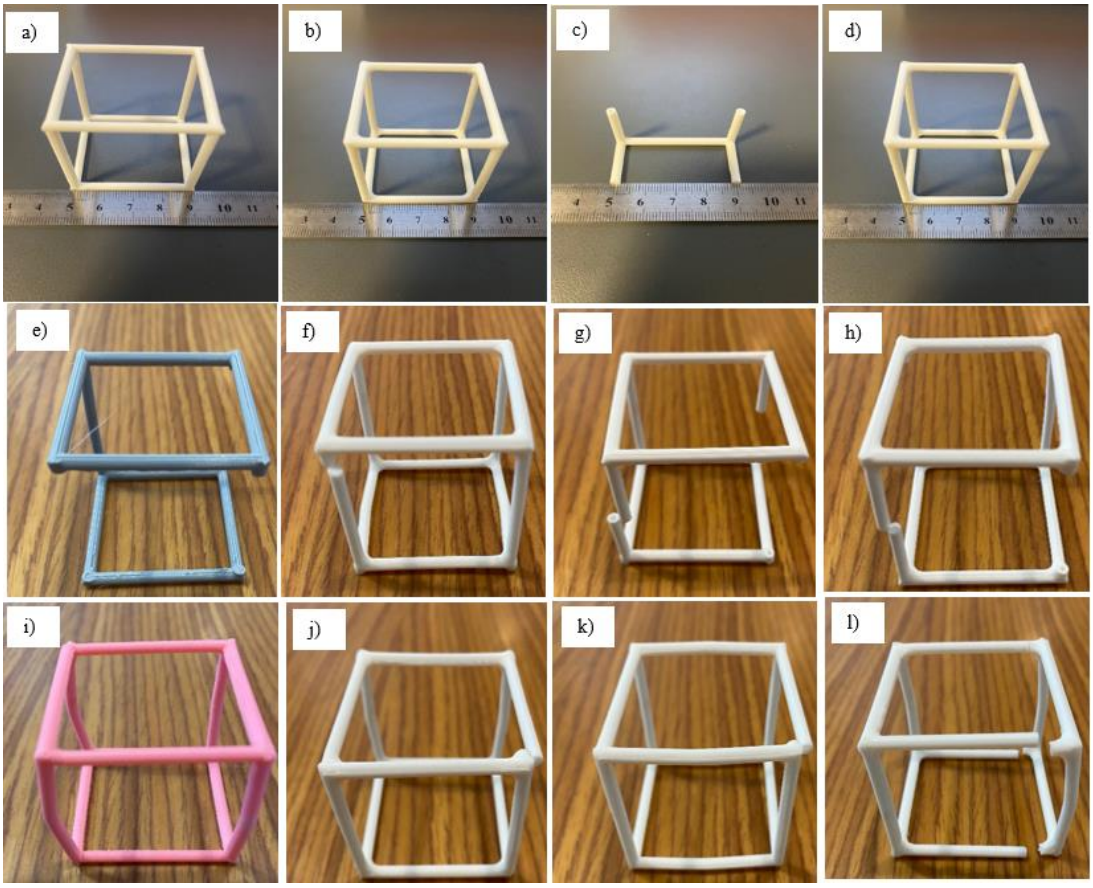

Figure 4.10. a) SC-WR, b) SC-R, c) SC-WR-H, d) SC-R-H, e) SC-WR-MD failure, f) SC-R-M failure, g) SC-WR-H-M failure, h) SC-R-H-M failure, i) SC-WR-NM failure, j) SC-R-NM failure, k) SC-WR-H-NM failure, l) SC-R-H-NM failure

4.3 Mechanical testing of face-centered cubic lattices

In Figure 4.11, compression test results for face-centered cubic lattice according to manufacturing direction are given. Finite element simulations were done. Elastic modulus of samples and the UTS values turned out to be slightly different from each other.

In Figure 4.12, compression test results for face-centered cubic lattice according to non-manufacturing direction are given. In addition, finite element simulations were done for each parameter.

Tests which were done through non-manufacturing direction showed variations in terms of modulus of elasticity and UTS values when compared with manufacturing

direction. Furthermore, the results of finite element simulations were close to the results of the tests involving manufacturing direction.

The addition of radius on the face-centered cubic lattice increased the stiffness of structure. In Figure 4.11 and 4.12, strength and UTS point increase can be seen for radius parameter. According to the finite element analysis and tests, stress concentrated at the intersection nodes and failure began from these nodes (Kaur et al., 2017). Moreover, according to this result, addition of radius at the intersection point of face-centered cubic lattice increased the UTS point and stiffness of the cubic lattice structure.

According to the literature, lattices generally are investigated and analyzed under uniaxial compression loading condition (Molavitabrizi et al., 2022). In Equation 4.1, matrix formation of uniaxial loading condition is expressed.

$$\text{Uniaxial: } \begin{bmatrix} \in_{xx} & 0 & 0 \\ 0 & 0 & 0 \\ 0 & 0 & 0 \end{bmatrix} \tag{4.1}$$

To predict out of plane displacement and stress values, $\in_{yy}$ and $\in_{zz}$ directions should be modeled. Because these two values are equal to zero, trusses cannot move in these directions and simulation program assumes that the truss structure in these directions are purely rigid. In this study, the addition of radius on trusses increased the strength of face-centered cubic lattice. However, radiuses cannot be modeled in the simulation program. On the other hand, radius effect on the structure was added in the material data section for finite element simulation program and this made it possible to predict displacement results more accurately.

In Figure 4.12, there are some differences between samples in terms of their UTS value and elastic modulus values. In literature, post buckling behavior of cubic lattices was studied using 3D meshing method for different types of cubic lattices under compressive loading conditions (Derveni et al., 2022). In this study, post buckling mechanical failure modes were not studied and the differences between the results of the finite element model and those of the compression tests were as expected.

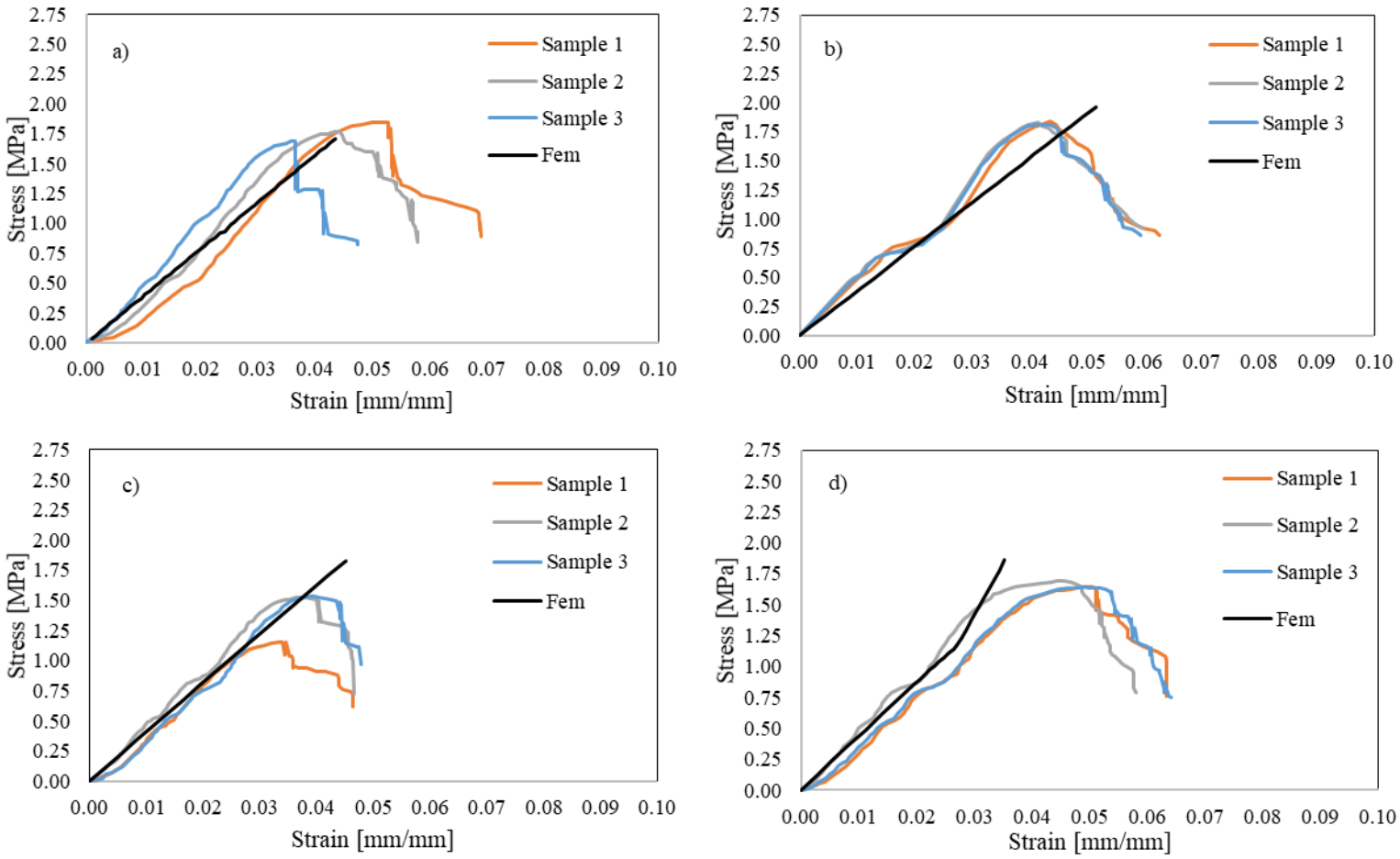

Figure 4.11. Compression test results of a) FC-WR-M, b) FC-R-M, c) FC-WR-H-M, d) FC-R-H-M

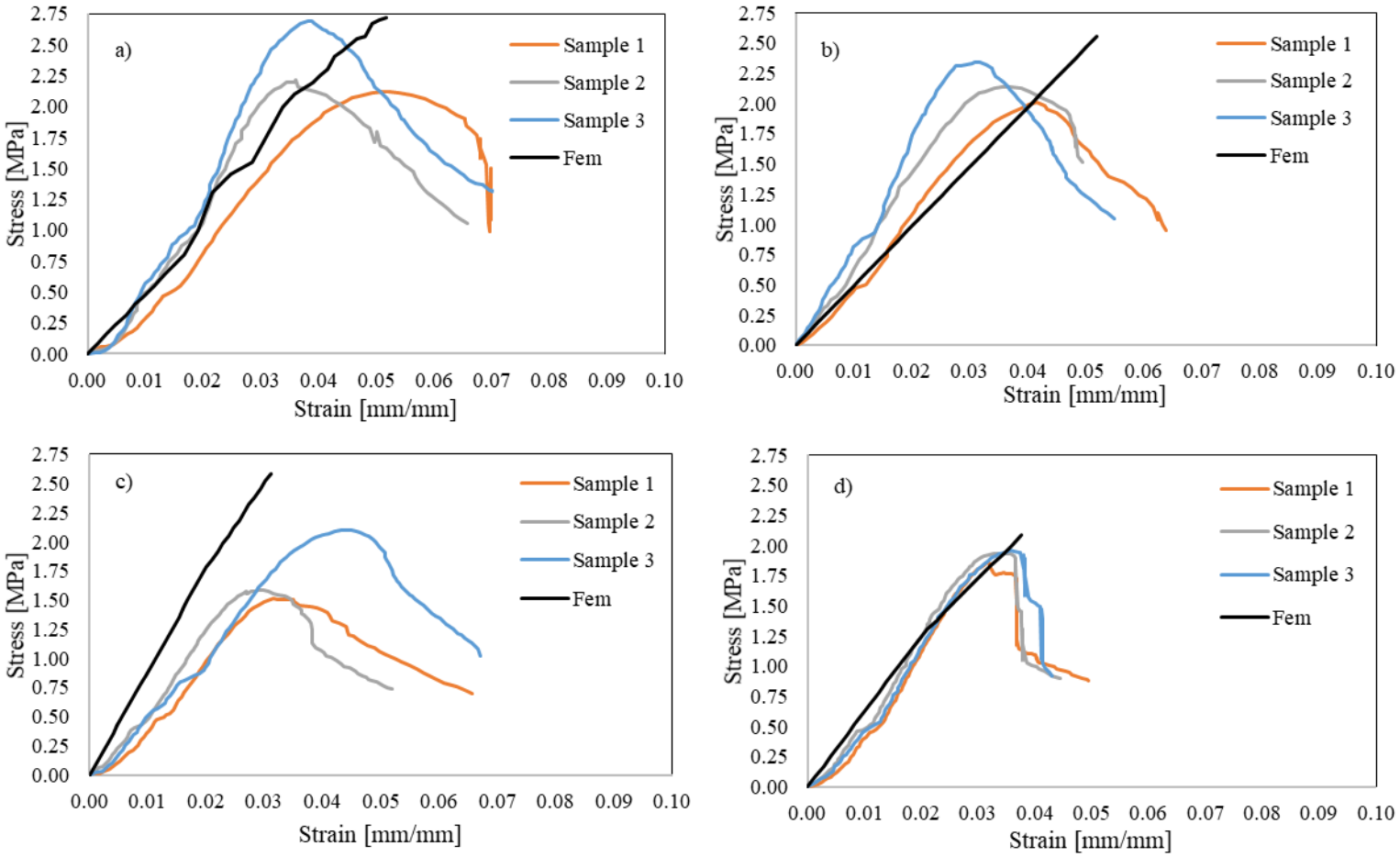

Figure 4.12. Compression test results of a) FC-WR-NM, b) FC-R-NM, c) FC-WR-H-NM, d) FC-R-H-NM

In Table 4.2, face-centered cubic lattice structure UTS and weight values are compared with without radius parameter and strength increase or decrease percentages and weight reduction values are calculated.

Firstly, tests were done through manufacturing direction of face-centered cubic lattice structures, and strength and weight reduction values were calculated. As can be seen from Table 4.2, when radii were added at the junction point of trusses, strength value increased by 3.21% from without radius parameter to with radius parameter. Also, the addition of radii on trusses increased the weight of face-centered cubic lattice structure by 3.04%. Furthermore, removing material from the truss centers decreased the strength by 13.90% from without radius parameter to hollow truss parameter. Moreover, removing material from the center of trusses decreased the weight by 14.37%. To increase the strength of structure for hollow truss, radii were added at the junction point of trusses. When WR parameter is compared with R-H parameter, it is observed that strength decreased by 8.02% and weight decreased by 13.97%.

Secondly, tests were done according to the non-manufacturing direction of face-centered cubic lattice structure, and strength and weight reduction values were calculated. Although addition of radii at the junction point of trusses increased the strength value of cubic lattices in manufacturing direction parameter, it did not increase it regarding the non-manufacturing direction parameter. The addition of radii decreased the strength by 4.51% from without radius parameter to radius parameter. Also, weight increased by 3.04% from without radius parameter to radius parameter. Removing the material from the center of trusses decreased the strength value by 32.79% and the weight value decreased by 14.37%. Hollow truss and radius parameter decreased the strength by 16.80% and decreased the weight of face-centered cubic lattice by 13.97%.

Table 4.2. Strength and weight reduction rate calculation for face-centered cubic lattices

Manuf direction	Manufacturing direction of samples				None manufacturing direction of samples			
Type of parameter	WR	R	WR-H	R-H	WR	R	WR-H	R-H
Sigma_UTS [MPa]	1.87	1.93	1.61	1.72	2.44	2.33	1.64	2.03
Weight [g]	9.88	10.18	8.46	8.50	9.88	10.18	8.46	8.50
Strength R, WR-H, R-H vs WR [%]	-	3.21	-13.90	-8.02	-	-4.51	-32.79	-16.80
Weight R, WR-H, R-H vs WR [%]	-	3.04	-14.37	-13.97	-	3.04	-14.37	-13.97

In Figure 4.13, face-centered cubic lattice finite element modeling displacement results are shown. Displacement and stress values changed according to the material properties which were obtained from mechanical compression tests. Face-centered cubic lattice was displaced 1.70 mm through z direction. Stress and strain diagrams for each parameter are shown in Figure 4.11 and Figure 4.12.

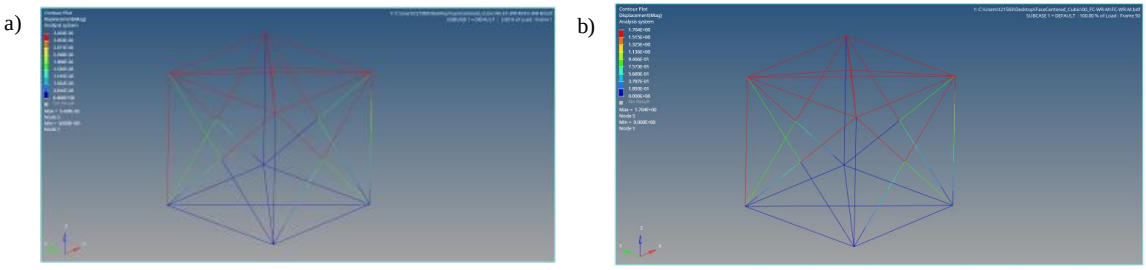

Figure 4.13. a) FC FEM modeling before compression load, b) FC FEM modeling after compression load

In Figure 4.14, before, during and after stages of the mechanical compression test of simple cubic lattice can be seen. The vertical truss structures of simple cubic lattice were buckled and after buckling failure trusses could not transfer load from the upper section to the lower section, and the bottom and upper sections of trusses were caused to fail by shear forces.

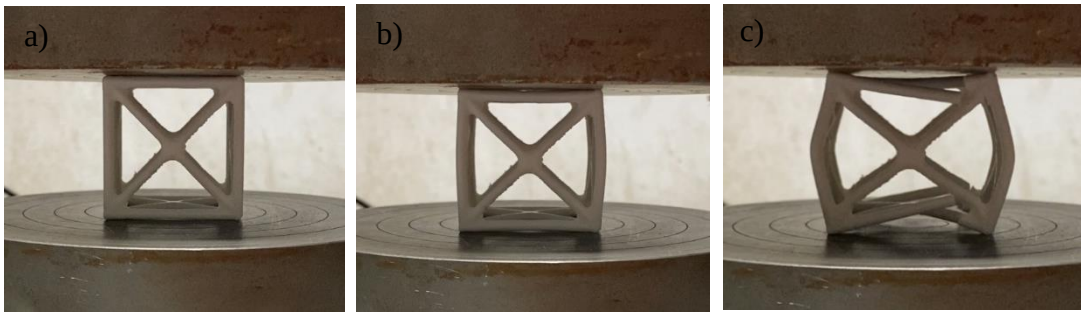

Figure 4.14. a) FC before the test, b) FC during the test, d) FC after the test

In Figure 4.15, the first eigenvalue for face-centered cubic lattice is shown. Buckling analysis was done using Nastran 105 solver. The first eigenvalue for face-centered cubic lattice is 0.836, which means face-centered cubic lattice was buckled under 84% of quasi static compression load. After that phenomenon, vertical trusses could not transfer load from the upper section to the lower section and horizontal trusses were made to fail by shear forces.

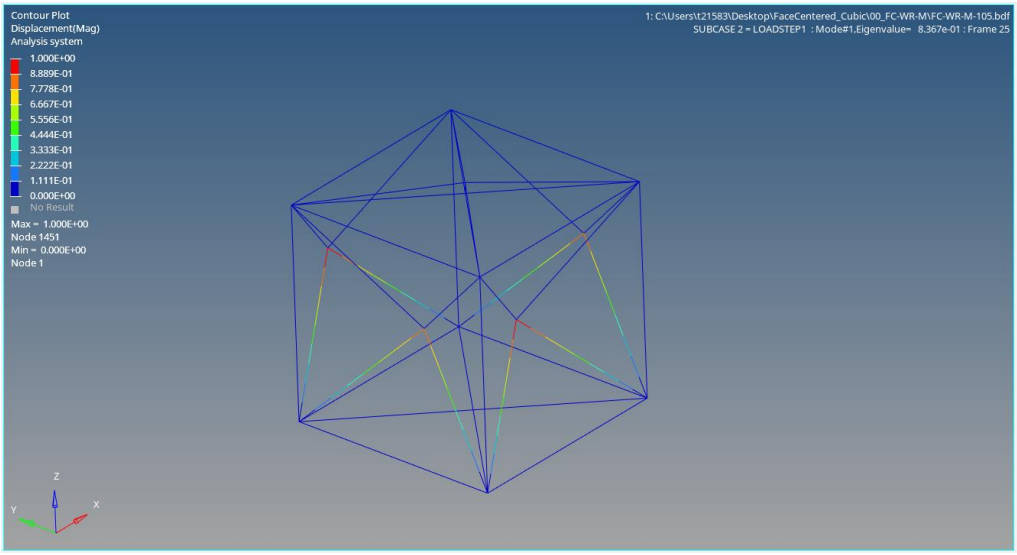

Figure 4.15. FC first eigenvalue mode

In Figure 4.16, the second eigenvalue mode of face-centered cubic lattice is shown. Eigenvalue is 0.836, which means that face-centered cubic lattice was buckled under 84% of quasi static compression load. The first and second eigenvalue is the same for face-centered cubic lattice. However, displacements are different from each other and this results from geometrical conditions.

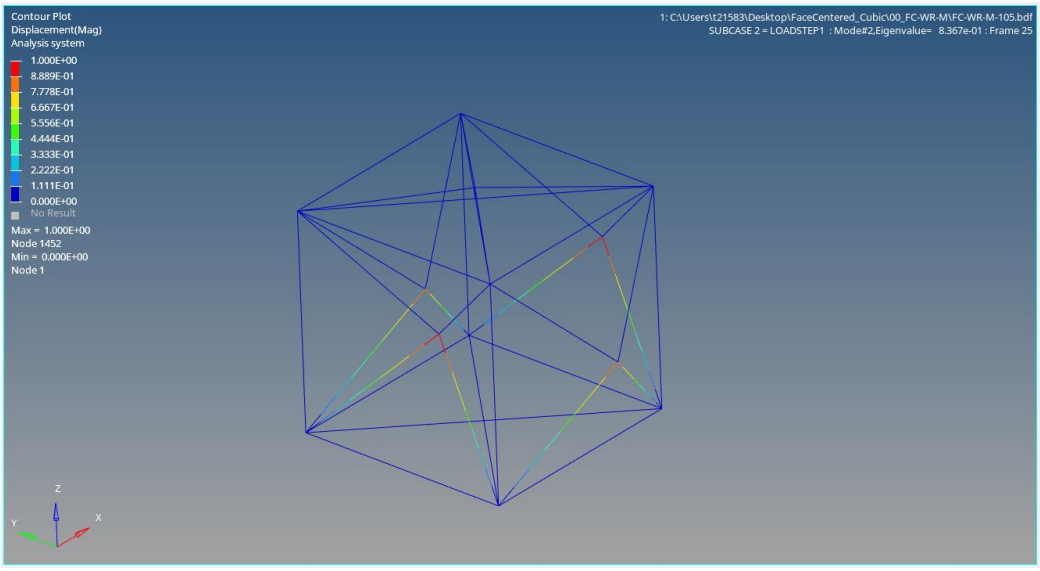

Figure 4.16. FC second eigenvalue mode

In Figure 4.17, the third eigenvalue mode of face-centered cubic lattice is shown. The eigenvalue is 0.837, which means face-centered cubic lattice was buckled under 84% of quasi static compression load.

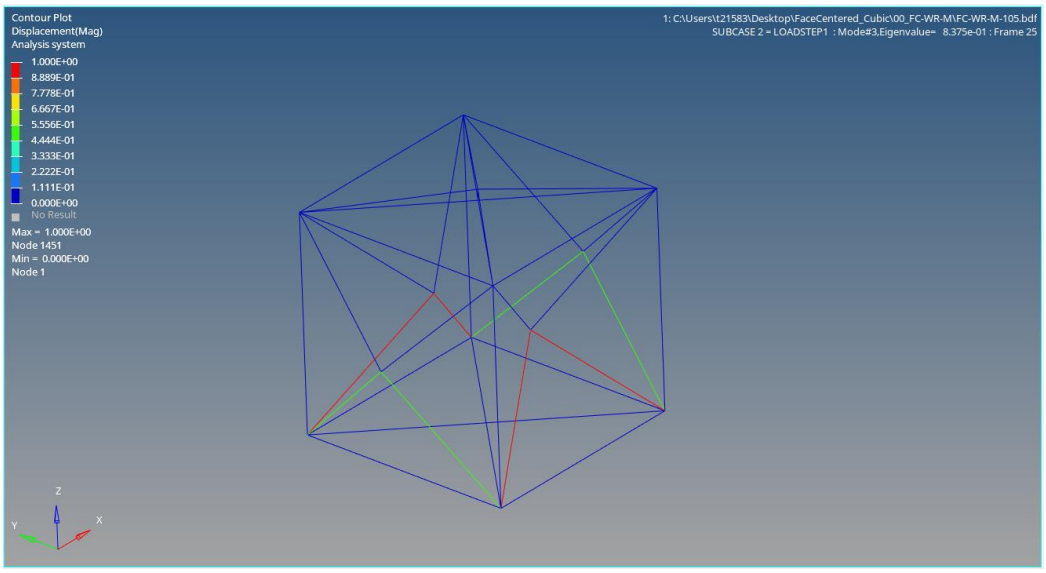

Figure 4.17. FC third eigenvalue mode

In Figure 4.18, the fourth eigenvalue mode of face-centered cubic lattice is shown. The eigenvalue is 0.837, which means face-centered cubic lattice was buckled under 84% of quasi static compression load. The third and fourth eigenvalue of face-centered cubic lattice is the same. However, displacements of trusses are different from each other because of geometrical variations.

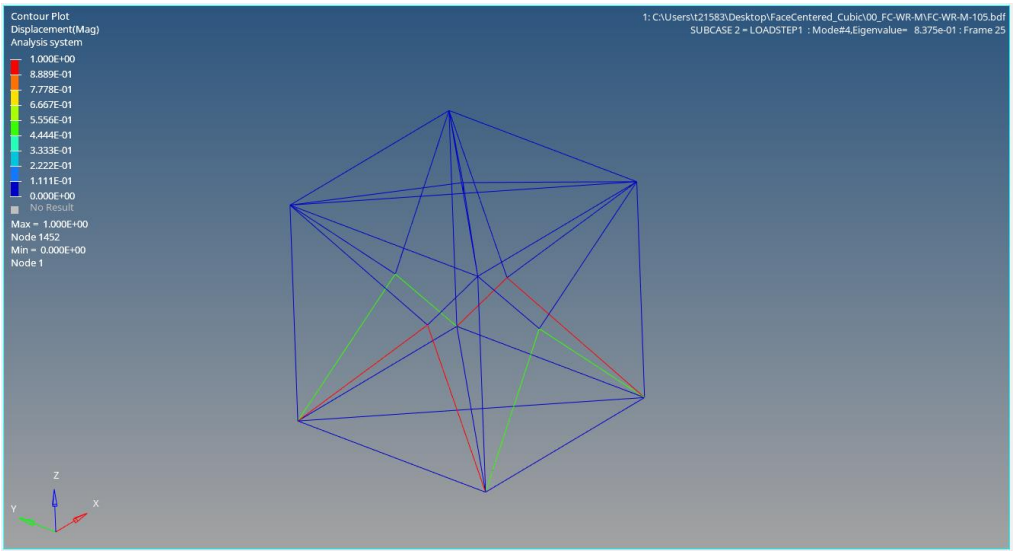

Figure 4.18. FC fourth eigenvalue mode

In Figure 4.19, face-centered cubic failure and before failure modes can be seen. Failure modes change according to the compression tests which were done through manufacturing direction or non-manufacturing direction of face-centered cubic lattices.

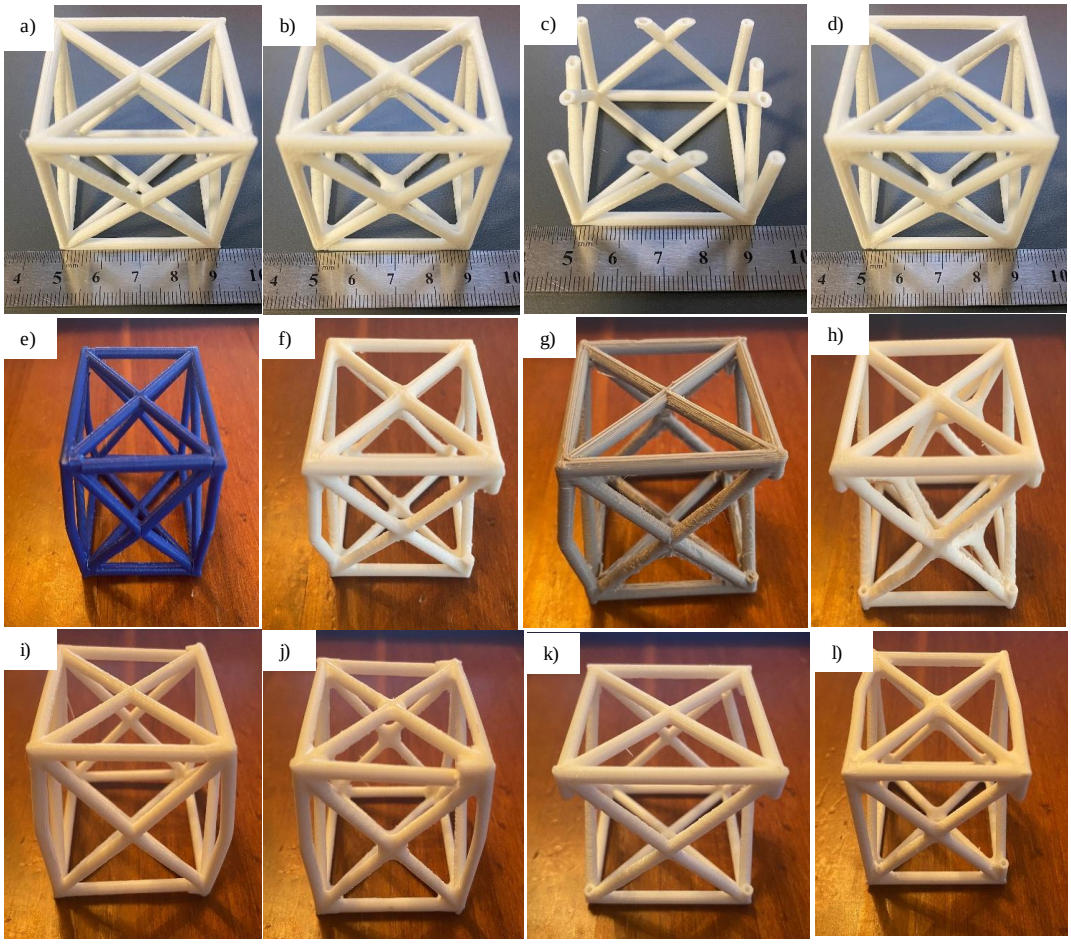

Figure 4.19. a) FC-WR, b) FC-R, c) FC-WR-H, d) FC-R-H, e) FC-WR-MD failure, f) FC-R-M failure, g) FC-WR-H-M failure, h) FC-R-H-M failure, i) FC-WR-NM failure, j) FC-R-NM failure, k) FC-WR-H-NM failure, l) FC-R-H-NM failure

4.4 Mechanical testing of diamond cubic lattices

In Figure 4.20, compression test results for the diamond cubic lattice according to manufacturing direction are given. Also, finite element analysis was done using material data obtained from mechanical compression tests. The UTS values are nearly the same for three different samples.

In Figure 4.21, compression test results for diamond cubic lattice according to non-manufacturing direction are given. Finite element analysis was done separately for different geometrical parameters. The UTS values are slightly different from each other because of the manufacturing direction of the diamond cubic lattices.

Consequently, tests done through manufacturing direction and tests done through non-manufacturing direction are different from each other in terms of mechanical properties. Moreover, samples tested according to manufacturing direction nearly have the same UTS values, while samples tested through non-manufacturing direction show some differences in terms of the UTS values.

Diamond cubic lattices are bending-dominated structures and face-centered cubic lattices are stretching-dominated ones. According to the literature, bending-dominated structures can carry more load than stretching-dominated structures under compressive loading conditions (Sun et al., 2021a). After mechanical compression tests, diamond cubic lattice UTS points turned out to be higher than face-centered cubic lattice UTS points for each parameter.

The second moment of area for solid trusses are higher than hollow trusses and the result is that solid trusses are stiffer than hollow trusses for diamond cubic lattices. In Figures 4.20 and 4.21, there are differences between the finite element model results and test results. Finite element models use the beam theory, and 3D mesh yields more accurate results than 2D mesh (Moeini et al., 2022). In this study, all trusses used the beam theory with 1D element mesh and this resulted in the differences between simulations and mechanical compression tests.

In Figure 4.23, diamond cubic lattice was compressed through manufacturing direction of cubic lattice and middle nodes of diamond cubic lattice turned around

itself and these nodes were connected to inner four nodes. However, turning of middle section nodes for diamond cubic lattices could not be observed in finite element analysis results. To simulate the turning and out plane displacements, matrix form of finite element simulation should be in Equation 4.2.

$$\text{Multiaxial: } \begin{bmatrix} \in_{xx} & \in_{xy} & \in_{xz} \\ \in_{yx} & \in_{yy} & \in_{yz} \\ \in_{zx} & \in_{zy} & \in_{zz} \end{bmatrix} \tag{4.2}$$

$\in_{xy}$, $\in_{xz}$, $\in_{yx}$, $\in_{yz}$, $\in_{zx}$ and $\in_{zy}$ can detect the rotation of trusses at the middle section of diamond cubic lattices and they can detect the deformations of trusses at the inner sections. In this study, trusses were modeled as uniaxial matrix formations and because of that we were not able to simulate the rotations of trusses.

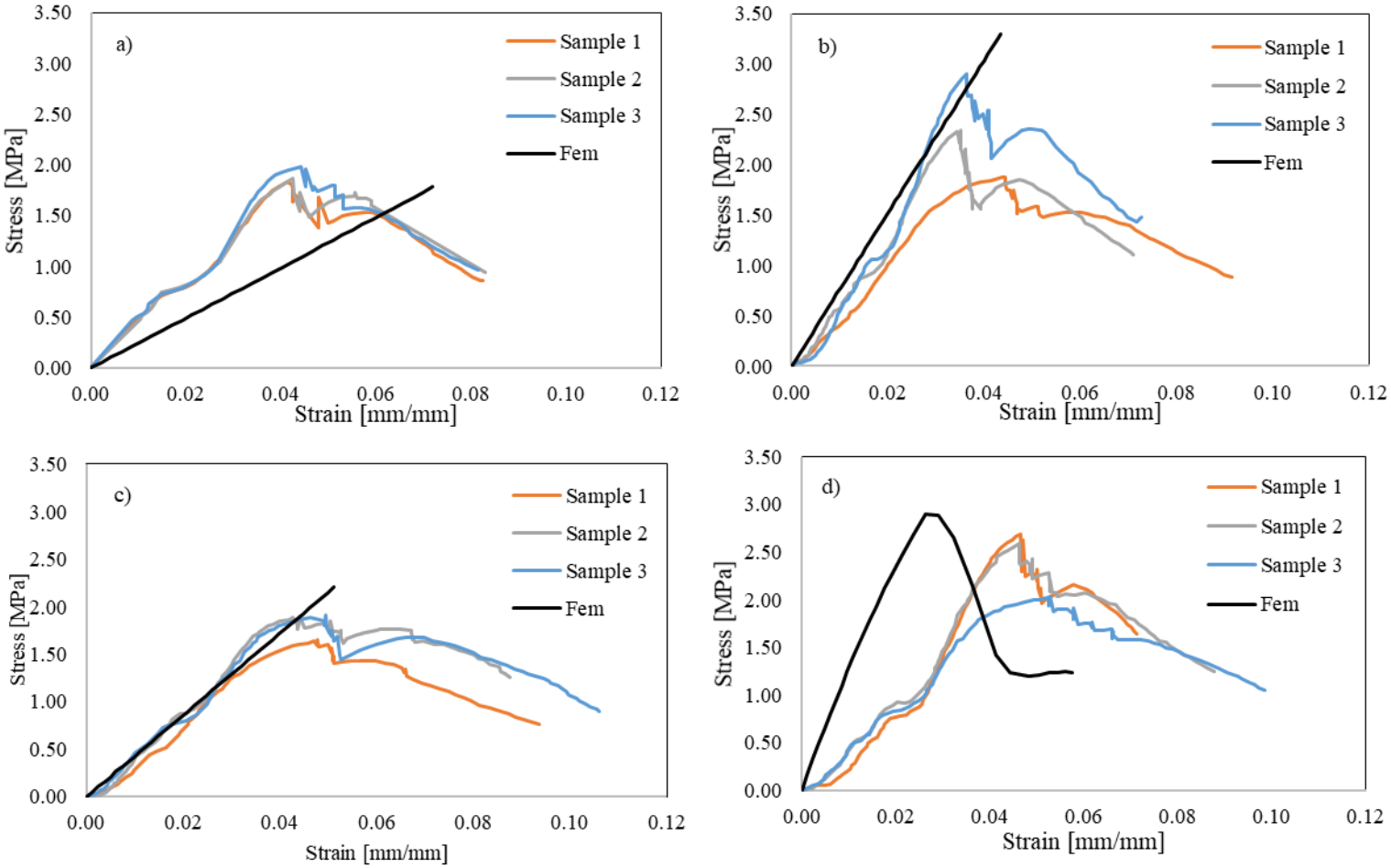

Figure 4.20. Compression test results of a) DC-WR-M, b) DC-R-M, c) DC-WR-H-M, d) DC-R-H-M

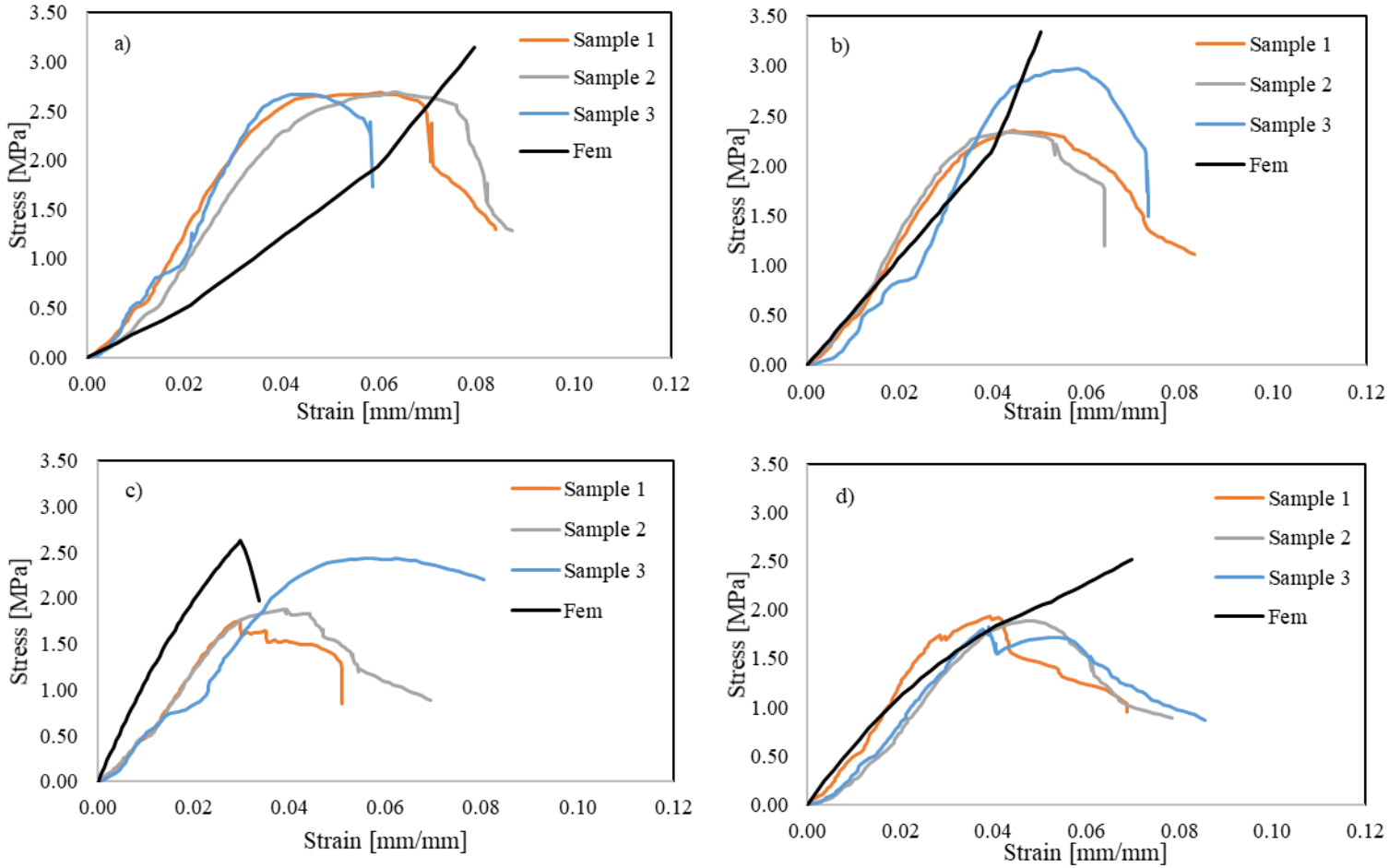

Figure 4.21. Compression test results of a) DC-WR-NM, b) DC-R-NM, c) DC-WR-H-NM, d) DC-R-H-NM

Table 4.3 shows the strength and weight reduction percentage calculations for both manufacturing and non-manufacturing directions of diamond cubic lattice. While calculating strength and weight reduction values, without radius parameter was selected as base parameter.

Firstly, strength and weight reduction calculations were done for the manufacturing direction parameter. The addition of radii on trusses increased the strength by 23.62% from without radius parameter to radius parameter and increased the weight of diamond cubic lattices by 2.30%. Moreover, removing the material from the center of trusses decreased the strength by 4.02%. Also, hollow truss parameter considerably decreased the weight by 12.94%. Furthermore, hollow truss and addition of radii at the trusses' junction point parameter increased the strength by 25.63% and slightly decreased the weight of the diamond cubic lattices by 0.43%.

Secondly, strength and weight reduction calculations were separately done for non-manufacturing direction of diamond cubic lattices since mechanical responses were changing according to the manufacturing direction of cubic lattices. Trusses which have radii on intersection points were less stiff than those that do not. The addition of radii decreased strength by 12.86%. For example, the addition of radius parameter increased the strength value for manufacturing direction parameter. Also, radii on trusses increased the weight by 2.30%. Furthermore, hollow truss parameter decreased the strength by 33.21% and decreased the weight by 12.94%. Moreover, hollow trusses with radius parameter decreased the strength by 30.36% and decreased the weight by 0.43% when compared with the without radius parameter of diamond cubic lattice.

Table 4.3. Strength and weight reduction rate calculation for diamond cubic lattices

Manuf direction	Manufacturing direction of samples				None manufacturing direction of samples			
Type of parameter	WR	R	WR-H	R-H	WR	R	WR-H	R-H
Sigma_UTS [MPa]	1.99	2.46	1.91	2.50	2.80	2.44	1.87	1.95
Weight [g]	11.75	12.02	10.23	11.70	11.75	12.02	10.23	11.70
Strength R, WR-H, R-H vs WR [%]	-	23.62	-4.02	25.63	-	-12.86	-33.21	-30.36
Weight R, WR-H, R-H vs WR [%]	-	2.30	-12.94	-0.43	-	2.30	-12.94	-0.43

In Figure 4.22, the diamond cubic lattice finite element models before and after uniaxial compression load results are shown. The diamond cubic lattice was displaced nearly 0.95 mm after compressive load. Stress-strain diagrams of diamond cubic lattices and other parameters are shown in Figure 4.20 and Figure 4.21.

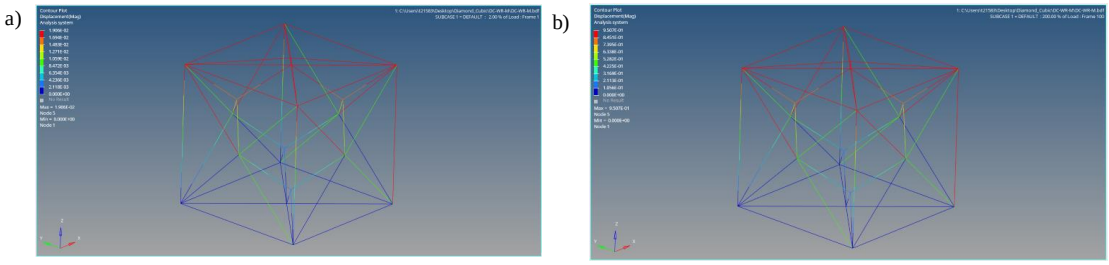

Figure 4.22. a) DC FEM modeling before compression load, b) DC FEM modeling after compression load

In Figure 4.23, before, during and after stages of the mechanical compression test for the diamond cubic lattice can be seen. The vertical truss structures of the diamond cubic lattice were buckled and after buckling, trusses could not transfer the load from the upper section to the lower section. After vertical trusses buckled, the center point of diamond cubic lattice structures turned around itself.

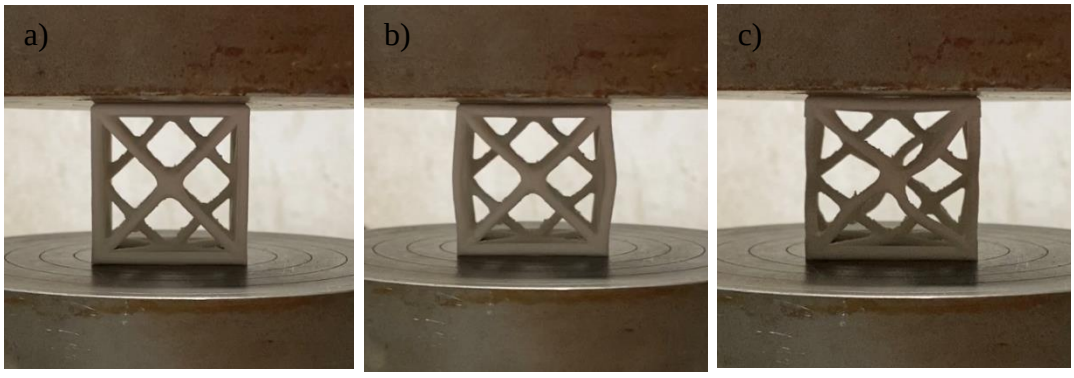

Figure 4.23. a) DC before the test, b) DC during the test, d) DC after the test

In Figure 4.24, the eigenvalue mode of the diamond cubic lattice is shown. The eigenvalue for the diamond cubic lattice was obtained using Nastran 105 buckling analysis solver. One eigenvalue was detected, which is 0.737. It means that diamond the cubic lattice was buckled under 74% of quasi static compression load.

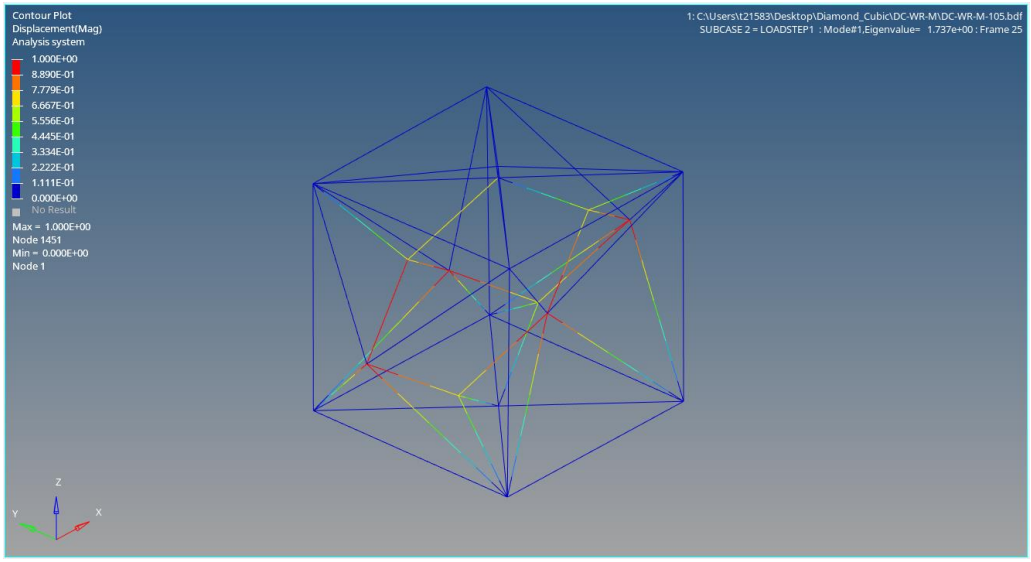

Figure 4.24. DC eigenvalue mode

In Figure 4.25, diamond cubic lattice failure modes can be seen. Compression tests done through manufacturing direction caused the trusses to break. However, non-manufacturing direction tests did not break off the truss since buckling behavior was observed on trusses.

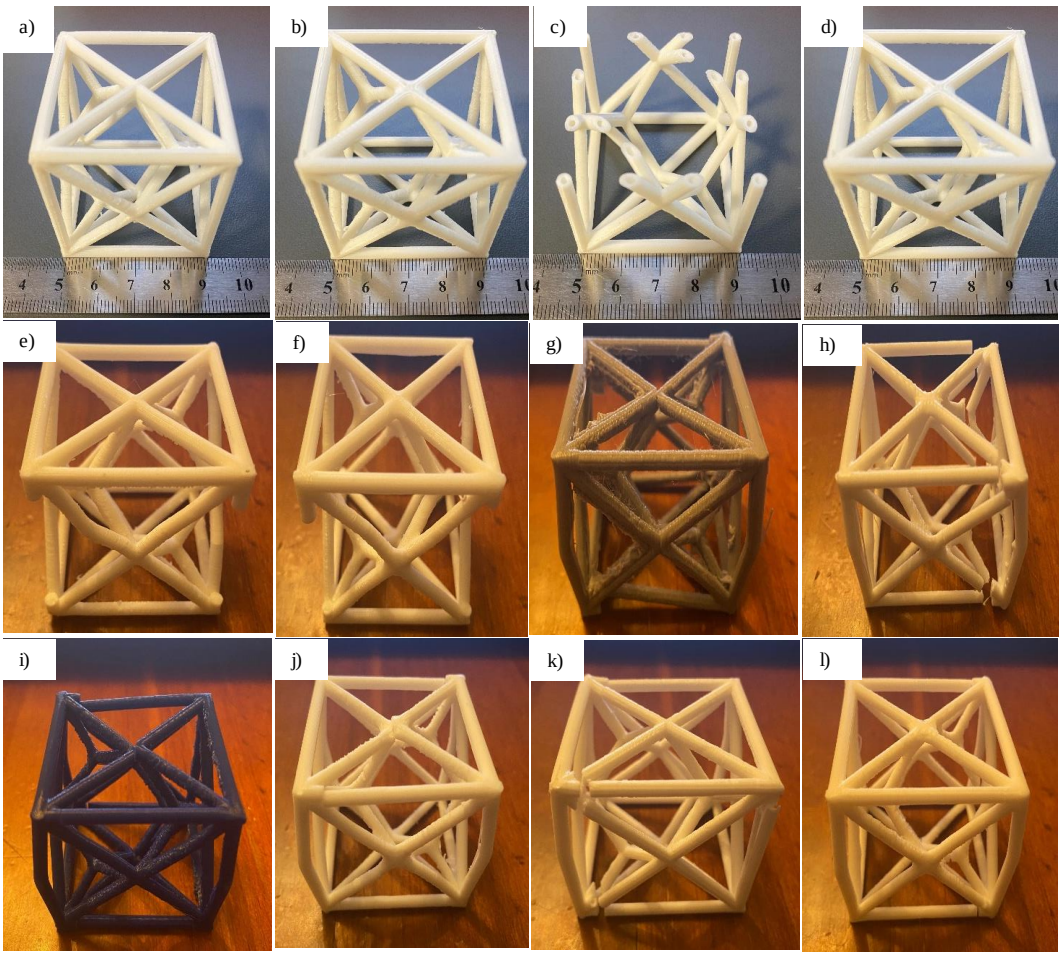

Figure 4.25. a) DC-WR, b) DC-R, c) DC-WR-H, d) DC-R-H, e) DC-WR-MD failure, f) DC-R-M failure, g) DC-WR-H-M failure, h) DC-R-H-M failure, i) DC-WR-NM failure, j) DC-R-NM failure, k) DC-WR-H-NM failure, l) DC-R-H-NM failure

CHAPTER 5

5. CONCLUSION

The following are the major findings of this thesis:

1. Simple, face-centered, and diamond cubic lattices can be produced by fused deposition modeling method. Adding radii at the corner of trusses and removing material from the center of trusses changed the mechanical properties of cubic lattices under uniaxial compression loading condition. Moreover, manufacturing direction had a major effect on mechanical properties and tests show that changing the manufacturing direction dramatically affected mechanical failures under uniaxial compressive loads. Cubic lattice structures tested through manufacturing direction usually behaved in a brittle manner, while trusses of simple, face-centered, and diamond cubic lattices broke off. On the other hand, cubic lattices which were tested according to the non-manufacturing direction showed ductile material behavior. Trusses first were buckled and then broke, and this mechanical behavior changed the stress-strain diagrams. Furthermore, manufacturing direction tests appeared to be more convenient than non-manufacturing direction tests in terms of force and displacement diagrams since non-manufacturing direction test failures could occur in different eigenvalues of the buckling phenomenon.
2. Strength and weight reduction calculations were done for each parameter of simple, face-centered and diamond cubic lattices in terms of manufacturing and non-manufacturing direction, and calculations show that adding radii at the corner of the trusses increased the ultimate tensile point of cubic lattices under uniaxial compression loading condition. Strength increase was the most considerable change in the diamond cubic lattices which were tested through manufacturing direction. Also,

diamond cubic lattice turned out to be the most durable against compression load. Moreover, finite element modeling of cubic lattices was done using one dimensional element, CBAR, to achieve results more precisely and quickly since modeling the cubic lattices with three dimensional elements converge the results slowly. To obtain precise results from the simulations, nonlinear material and nonlinear geometric analysis type can be used since linear analysis methods cannot simulate beyond the yield point of materials.

Consequently, simple, face-centered and diamond cubic lattices which have without radius, with radius and hollow truss parameters were tested under uniaxial loading condition and finite element simulations were done to simulate the mechanical behavior of cubic lattices. As was revealed, the diamond cubic lattice with hollow truss parameter is the best performing one under uniaxial compression loading condition.

REFERENCES

Agarwal, P. K., Gupta, M. (2017). International Conference on Advances in Mechanical, Industrial, Automation and Management Systems (AMIAMS): Proceedings: February 3-5.

Ahn, S. H., Montero, M., Odell, D., Roundy, S., & Wright, P. K. (2002). Anisotropic material properties of fused deposition modeling ABS. *Rapid Prototyping Journal*, *8*(4), 248–257.

Attaran, M. (2017). The rise of 3-D printing: The advantages of additive manufacturing over traditional manufacturing. *Business Horizons*, *60*(5), 677–688.

Azzouz, L., Chen, Y., Zarrelli, M., Pearce, J. M., Mitchell, L., Ren, G., & Grasso, M. (2019). Mechanical properties of 3-D printed truss-like lattice biopolymer non-stochastic structures for sandwich panels with natural fibre composite skins. *Composite Structures*, *213*, 220–230.

Bikas, H., Stavropoulos, P., & Chryssolouris, G. (2016). Additive manufacturing methods and modeling approaches: A critical review. *International Journal of Advanced Manufacturing Technology*, *83*(1–4), 389–405.

Bonatti, C., & Mohr, D. (2019). Smooth-shell metamaterials of cubic symmetry: Anisotropic elasticity, yield strength and specific energy absorption. *Acta Materialia*, *164*, 301–321.

Bourell, D., Kruth, J. P., Leu, M., Levy, G., Rosen, D., Beese, A. M., & Clare, A. (2017). Materials for additive manufacturing. *CIRP Annals - Manufacturing Technology*, *66*(2), 659–681.

Derveni, F., Gross, A. J., Peterman, K. D., & Gerasimidis, S. (2022). Postbuckling behavior and imperfection sensitivity of elastic–plastic periodic plate-lattice materials. *Extreme Mechanics Letters*, *50*,101510.

Dong, J., Wang, Y., Jin, F., & Fan, H. (2021). Crushing behaviors of buckling-induced metallic meta-lattice structures. *Defence Technology*, *18*(7), 1097-1280.

Fernandes, R. R., & Tamijani, A. Y. (2021). Design optimization of lattice structures with stress constraints. *Materials and Design*, *210*, 110026.

Helou, M., & Kara, S. (2018). Design, analysis, and manufacturing of lattice structures: An overview. *International Journal of Computer Integrated Manufacturing*, *31*(3), 243–261.

Hoang, V. N., Tran, P., Vu, V. T., & Nguyen-Xuan, H. (2020). Design of lattice structures with direct multiscale topology optimization. *Composite Structures*, *252*, 112718.

Karamooz Ravari, M. R., Kadkhodaei, M., Badrossamay, M., & Rezaei, R. (2014). Numerical investigation on mechanical properties of cellular lattice structures fabricated by fused deposition modeling. *International Journal of Mechanical Sciences*, *88*, 154–161.

Kaur, M., Yun, T. G., Han, S. M., Thomas, E. L., & Kim, W. S. (2017). 3D printed stretching-dominated micro-trusses. *Materials and Design*, *134*, 272–280.

Maconachie, T., Leary, M., Lozanovski, B., Zhang, X., Qian, M., Faruque, O., & Brandt, M. (2019). SLM lattice structures: Properties, performance, applications, and challenges. *Materials & Design*, *183*, 108137.

Moeini, M., Begon, M., & Lévesque, M. (2022). Numerical homogenization of a linearly elastic honeycomb lattice structure and comparison with analytical and experimental results. *Mechanics of Materials*, *167*, 104210.

Mofokeng, J. P., Luyt, A. S., Tábi, T., & Kovács, J. (2012). Comparison of injection moulded, natural fibre-reinforced composites with PP and PLA as matrices. *Journal of Thermoplastic Composite Materials*, *25*(8), 927–948.

Molavitabrizi, D., Bengtsson, R., Botero, C., Rännar, L.-E., & Mahmoud Mousavi, S. (2022). Damage-induced failure analysis of additively manufactured lattice materials under uniaxial and multiaxial tension. *International Journal of Solids and Structures*, *252*, 111783.

Murariu, M., Bonnaud, L., Yoann, P., Fontaine, G., Bourbigot, S., & Dubois, P. (2010). New trends in polylactide (PLA)-based materials: "Green" PLA-Calcium sulfate (nano)composites tailored with flame retardant properties. *Polymer Degradation and Stability*, *95*(3), 374–381.

Ozdemir, Z., Hernandez-Nava, E., Tyas, A., Warren, J. A., Fay, S. D., Goodall, R., Todd, I., & Askes, H. (2016). Energy absorption in lattice structures in dynamics: Experiments. *International Journal of Impact Engineering*, *89*, 49–61.

Pan, C., Han, Y., & Lu, J. (2020). Design and optimization of lattice structures: A review. *Applied Sciences (Switzerland)*, *10* (18), 1-36.

Peng, C., Tran, P., Nguyen-Xuan, H., & Ferreira, A. J. M. (2020). Mechanical performance and fatigue life prediction of lattice structures: Parametric computational approach. *Composite Structures*, *235*, 111821.

Pereira, T., Kennedy, J. V., & Potgieter, J. (2019). A comparison of traditional manufacturing vs additive manufacturing, the best method for the job. *Procedia Manufacturing*, *30*, 11–18.

Sallica-Leva, E., Caram, R., Jardini, A. L., & Fogagnolo, J. B. (2016). Ductility improvement due to martensite α' decomposition in porous Ti-6Al-4V parts produced by selective laser melting for orthopedic implants. *Journal of the Mechanical Behavior of Biomedical Materials*, *54*, 149–158.

Savio, G., Rosso, S., Meneghello, R., & Concheri, G. (2018). Geometric modeling of cellular materials for additive manufacturing in biomedical field: A review. *In Applied Bionics and Biomechanics*, 2018, 1-14.

Sun, Z. P., Guo, Y. B., & Shim, V. P. W. (2021a). Characterisation and modeling of additively-manufactured polymeric hybrid lattice structures for energy absorption. *International Journal of Mechanical Sciences*, *191*, 106101.

Sun, Z. P., Guo, Y. B., & Shim, V. P. W. (2021b). Deformation and energy absorption characteristics of additively-manufactured polymeric lattice structures — Effects of cell topology and material anisotropy. Thin-Walled Structures, 169, 108420.

Tancogne-Dejean, T., & Mohr, D. (2018a). Elastically-isotropic truss lattice materials of reduced plastic anisotropy. *International Journal of Solids and Structures*, *138*, 24–39.

Tancogne-Dejean, T., & Mohr, D. (2018b). Elastically-isotropic elementary cubic lattices composed of tailored hollow beams. *Extreme Mechanics Letters*, *22*, 13–18.

Wu, J., Wang, W., & Gao, X. (2021). Design and optimization of conforming lattice structures. *IEEE Transactions on Visualization and Computer Graphics*, *27*(1), 43–56.

Zhou, X., Qu, C., Luo, Y., Heise, R., & Bao, G. (2021). Compression behavior and impact energy absorption characteristics of 3D printed polymer lattices and their hybrid sandwich structures. *Journal of Materials Engineering and Performance*, *30*(12), 8763–8770.